Synthesis, Structure, and Solution Dynamics of Neutral Allylnickel Complexes of N-Heterocyclic Carbenes

Leonel C. Silva,[†] Pedro T. Gomes,*[,†] Luis F. Veiros,[†] Sofia I. Pascu,[‡] M. Teresa Duarte,[†] Sónia Namorado,[†] José R. Ascenso,[†] and Alberto R. Dias[†]

Centro de Química Estrutural, Departamento de Engenharia Química, Instituto Superior Técnico, Av. Rovisco Pais, 1049-001 Lisboa, Portugal, and Chemistry Research Laboratory, University of Oxford, OX1 2TA Oxford, U.K.

Received May 19, 2006

Neutral allylnickel complexes of the general formula [Ni(η^3-C_3H_5)(Im)Br] (where Im = 1,3-di-*tert*-butylimidazol-2-ylidene ($^tBu_2$Im), 1,3,4,5-tetramethylimidazol-2-ylidene (Me_4Im), 1,3-dimethylimidazol-2-ylidine (Me_2Im)) were prepared from the reaction of the dimer [Ni(η^3-C_3H_5)Br]$_2$ with 2 equiv of the corresponding free N-heterocyclic carbene (NHC). The halide exchange of Br^- by I^- can be easily performed, giving rise to compounds of the type [Ni(η^3-C_3H_5)(Im)I]. The new complexes [Ni(η^3-C_3H_5)($^tBu_2$Im)Br] (**1**), [Ni(η^3-C_3H_5)(Me_4Im)Br] (**2**), [Ni(η^3-C_3H_5)(Me_2Im)Br] (**3**), [Ni(η^3-C_3H_5)(Me_2Im)I] (**4**), and [Ni(η^3-C_3H_5)(Me_4Im)I] (**5**) were obtained in good yields and were fully characterized by elemental analysis and NMR spectroscopy. The X-ray crystal structures of **1**, **2**, **4**, and **5** reveal a square-planar geometry at the nickel atom and a tilt angle of the NHC ring (in relation to the Ni square plane) dependent on the bulkiness of both the N substituents and the halogen bound to Ni. Variable-temperature NMR experiments in solution show that compounds **1**−**5** are stereochemically nonrigid. Three simultaneous dynamic processes are observed with increasing temperature: (a) NHC rotation about the nickel−carbon bond, starting at lower temperatures ($\Delta G^{\ddagger}$ = 14−18 kcal mol^{-1} for compounds **2**−**5**), (b) allyl rotation about the Ni−η^3-allyl axis, which is responsible for the cis−trans isomerization observed at intermediate temperatures ($\Delta G^{\ddagger}$ = 16.4 kcal mol^{-1} for compound **4**), and (c) $\pi-\sigma-\pi$ allyl isomerization, occurring at higher temperatures. DFT calculations were performed in order to elucidate the possible mechanisms involved and suggest (1) NHC rotation is mainly controlled by steric factors imposed by the N-substituent groups and to a lesser extent by the halogen and (2) there is a "spin-forbidden" mechanism for η^3-allyl rotation, involving spin singlet and triplet species. Thermodynamic activation parameters obtained by DFT agree well with the experimental values.

Introduction

The history of metal−carbene chemistry begins in 1964, with the work of Fischer and Maasböl.[1] A large number of applications for these compounds emerged early on, in both synthesis and catalysis.[2] In 1968, Wanzlick and Öfele reported stable mercury and chromium complexes bearing N-heterocyclic carbenes (NHC) or imidazol-2-ylidenes, derived from imidazolium salts.[3,4] This class of ligands became popular among organometallic chemists after Arduengo announced the synthesis and isolation of the first stable N-heterocyclic carbene, in 1991.[5] Herrmann and Köcher initiated their rich coordination and catalysis chemistry, based on similar properties between these compounds and electron-rich phosphines.[1,2] In general, imidazol-2-ylidenes are stronger Lewis bases and have reduced π back-bonding with respect to tertiary phosphines.[6] As a consequence, NHC complexes are more stable toward dissociation and degradative cleavage.[7,8] There have been a large number of publications revealing interesting catalytic properties of NHC complexes.[2,9−11] These complexes have been tested as catalysts for reactions such as C−C and C−N coupling,[12−15] ethylene and CO copolymerization,[16] hydrogenation, hydroformylation, and olefin metathesis.[1,2,17,18] In particular, [Pd(η^3-C_3H_5)(Im)-Cl] species (where Im stands for the imidazol-2-ylidenes with

* To whom correspondence should be addressed. E-mail: pedro.t.gomes@ist.utl.pt. Tel: +351 218419612. Fax: +351 218419612.
† Instituto Superior Técnico.
‡ University of Oxford.

(1) Herrmann, W. A.; Köcher, C. *Angew. Chem., Int. Ed.* **1997**, *36*, 2162.
(2) Herrmann, W. A. *Angew. Chem., Int. Ed.* **2002**, *41*, 1290.
(3) Öfele, K. *J. Organomet. Chem.* **1968**, *12*, P42.
(4) Wanzlick, H.-W.; Schönherr, H.-J. *Angew. Chem., Int. Ed. Engl.* **1968**, *7*, 141.
(5) Arduengo, A. J.; Harlow, R. F.; Kline, M. *J. Am. Chem. Soc.* **1991**, *113*, 361.
(6) Herrmann, W. A.; Goossen, L. J.; Spiegler, M. *J. Organomet. Chem.* **1997**, *547*, 357.
(7) Arnold, P. L.; Cloke, F. G. N.; Geldbach, T.; Hitchcock, P. B. *Organometallics* **1999**, *18*, 3228.
(8) Weskamp, T.; Böhm, V. P. W.; Herrmann, W. A. *J. Organomet. Chem.* **2000**, *600*, 12.
(9) McGuinness, D. S.; Mueller, W.; Wasserscheid, P.; Cavell, K. J.; Skelton, B. W.; White, A. H.; Englert, U. *Organometallics* **2002**, *21*, 175.
(10) Jackstell, R.; Andreu, M. G.; Frisch, A.; Selvakumar, K.; Zapf, A.; Klein, H.; Spannenberg, A.; Röttger, D.; Briel, O.; Karch, R.; Beller, M. *Angew. Chem., Int. Ed.* **2002**, *41*, 986.
(11) Viciu, M. S.; Germaneau, R. F.; Navarro-Fernandez, O.; Stevens, E. D.; Nolan, S. P. *Organometallics* **2002**, *21*, 5470.
(12) Caddick, S.; Cloke, F. G. N.; Clentsmith, G. K. B.; Hitchcock, P. B.; McKerrecher, D.; Titcomb, L. R.; Williams, M. R. V. *J. Organomet. Chem.* **2001**, *617*−*618*, 635.
(13) Viciu, M. S.; Zinn, F. K.; Stevens, E. D.; Nolan, S. P. *Organometallics* **2003**, *22*, 3175.
(14) Viciu, M. S.; Navarro, O.; Germaneau, R. F.; Kelly, R. A., III; Sommer, W.; Marion, N.; Stevens, E. D.; Cavallo, L.; Nolan, S. P. *Organometallics* **2004**, *23*, 1629.
(15) Titcomb, L. R.; Caddick, S.; Cloke, F. G. N.; Wilson, D. J.; McKerrecher, D. *Chem. Commun.* **2001**, 1388.
(16) Gardiner, M. G.; Herrmann, W. A.; Reisinger, C.; Schwarz, J.; Spiegler, M. *J. Organomet. Chem.* **1999**, *572*, 239.

10.1021/om060444p CCC: $33.50
Publication on Web 07/27/2006

Scheme 1. Syntheses of [Ni(η^3-C_3H_5)(Im)X] Compounds[a]

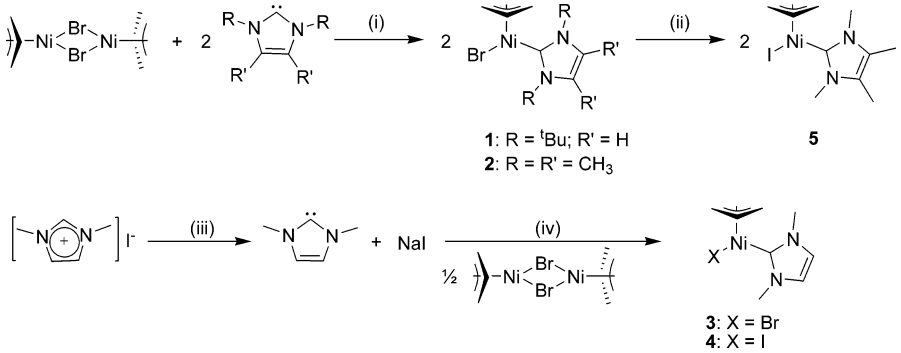

[a] Legend: (i) in THF, −50 °C to room temperature; (ii) NaI (excess), in THF, room temperature; (iii) NaH (10% excess), KO^{t}Bu (cat.), in THF, −80 °C to room temperature; (iv) for **3**, NHC extraction with toluene, then reaction with [Ni(η^3-C_3H_5)Br]$_2$, in THF, −50 °C to room temperature; for **4**, NHC extraction with THF, then reaction with [Ni(η^3-C_3H_5)Br]$_2$, in THF, −50 °C to room temperature.

different substituent groups on the nitrogen atoms) proved to be very useful reagents in cross-coupling reactions.[11,14] Similar complexes were reported by Ding et al.[19] In 2002, Dible and Sigman published the only article that describes nickel compounds of the type [Ni(η^3-allyl)(Im)Cl] (allyl = C_3H_5, 1-PhC_3H_4; Im = 1,3-bis(2,6-diisopropylphenyl)imidazol-2-ylidene) and reported their use as intermediates in the study of stoichiometric activation and splitting of molecular oxygen.[20]

It is known that ligand-stabilized allylnickel(II) halides, [Ni(η^3-allyl)(L)X] (X = Cl, Br, I; L = PR_3, $P(OR)_3$), act as very efficient catalysts for oligo-/polymerization of olefins and dienes in the presence of suitable Lewis acids.[21] Therefore, nickel complexes containing NHC ligands have potential interest as catalysts for these types of reactions.

The rotational fluxionality of the NHC ligands has scarcely been studied.[6,17,22] Also, the allyl ligand fluxionality has always been a matter of debate[23−25] and has been frequently associated with the initiation steps of catalytic reactions of allyl complexes.

In this work, we describe the synthesis of complexes of the type [Ni(η^3-C_3H_5)(Im)X], where Im = 1,3-dialkylimidazol-2-ylidenes and X = Br, I, and their corresponding solid-state and solution characterizations. We will particularly focus on the dynamic processes observed in solution: (a) the rotational fluxionality of the NHC ligand and (b) the allyl ligand fluxionality.

Results and Discussion

Synthesis of Complexes. The three imidazol-2-ylidenes used in this work (Chart 1), 1,3-di-*tert*-butylimidazol-2-ylidene (^{t}Bu$_2$Im), 1,3,4,5-tetramethylimidazol-2-ylidene (Me$_4$Im), and 1,3-dimethylimidazol-2-ylidine (Me$_2$Im), were obtained as described in the literature, by deprotonation of the corresponding imidazolium salts, using NaH and a catalytic amount of potassium *tert*-butoxide.[26] They were either isolated by crystallization (for ^{t}Bu$_2$Im and Me$_4$Im) or generated in situ (in the case of Me$_2$Im).

Chart 1

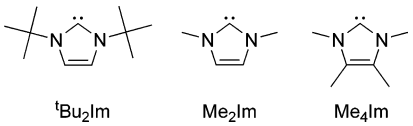

Neutral complexes of the general formula [Ni(η^3-C_3H_5)(Im)X] were prepared in good yields (72−89%) from the reaction of the dimer [Ni(η^3-C_3H_5)Br]$_2$ with 2 equiv of free NHC (Scheme 1).

We found that these reactions can be carried out in cold THF if the carbene of interest is previously isolated. The μ-Br bridge splitting by the carbene affords the correspondent monomeric bromide complexes **1** and **2**. However, if the deprotonation of the imidazolium iodide salt is made in situ, the resulting NaI remains partially soluble in THF. The addition of this mixture to a solution of the allylnickel bromide dimer in THF will result in the substitution of bromine by iodine, leading to the isolation of the corresponding iodide compound **4** (Scheme 1). To synthesize the bromide compound **3**, extraction of the free carbene had to be done in toluene, hence allowing the separation of all of the NaI from the following reaction step. This indicates that, as observed for similar Pd complexes,[19] the resulting Ni−I bond is stronger than the Ni−Br bond of the parent compound.

In fact, the treatment of these complexes with the adequate sodium halide salts, in THF, was shown to be a good method for halogen substitution. For instance, if an equimolar amount of NaI is added to a THF solution of **2** and stirred for 12 h, a mixture of [Ni(η^3-C_3H_5)(Me$_4$Im)I] (**5**) and unreacted [Ni(η^3-C_3H_5)(Me$_4$Im)Br] (**2**) is obtained after recrystallization. A yield of 66% for **5** was determined by ^{1}H NMR of the mixture. The spectrum had to be performed at low temperature (ca. 216 K), since broadening of the resonances was observed at room temperature, due to intermolecular exchange between **5** and **2**. To increase the yield in the synthesis of **5**, this mixture of compounds was further reacted with an excess of NaI for 36 h (final yield: 90%).

(17) Weskamp, T.; Schattenmann, W. C.; Spiegler, M.; Herrmann, W. A. *Angew. Chem., Int. Ed.* **1998**, *37*, 2490.
(18) Trnka, T. M.; Grubbs, R. H. *Acc. Chem. Res.* **2001**, *34*, 18.
(19) Ding, Y. Q.; Goddard, R.; Pörschke, K.-R. *Organometallics* **2005**, *24*, 439.
(20) Dible, B. R.; Sigman, M. S. *J. Am. Chem. Soc.* **2003**, *125*, 872.
(21) (a) Jolly, P. W.; Wilke, G. *The Organic Chemistry of Nickel*; Academic Press: New York, 1975; Vol. II. (b) Jolly, P. W. In *Comprehensive Organometallic Chemistry*; Wilkinson, G., Stone, F. G. A., Abel, E. W., Eds.; Pergamon: Oxford, U.K., 1982; Vol. 8.
(22) (a) Doyle, M. J.; Lappert, M. F. *J. Chem. Soc., Chem. Commun.* **1974**, 679. (b) Enders, D.; Gielen, H. *J. Organomet. Chem.* **2001**, *617−618*, 70. (c) Chianese, A. R.; Li, X.; Janzen, M. C.; Faller, J. W.; Crabtree, R. H. *Organometallics* **2003**, *22*, 1663. (d) Mata, J. A.; Chianese, A. R.; Miecznikowski, J. R.; Poyatos, M.; Peris, E.; Faller, J. W.; Crabtree, R. H. *Organometallics* **2004**, *23*, 1253.
(23) Vrieze, K. Fluxional Allyl Complexes. In *Dynamic Nuclear Magnetic Resonance Spectroscopy*; Jackman, L. M., Cotton, F. A., Eds.; Academic Press: New York, 1975; Chapter 11.
(24) Jalón, F. A.; Manzano, B. R.; Moreno-Lara, B. *Eur. J. Inorg. Chem.* **2005**, 100−109.
(25) Gogoll, A.; Örnebro, J.; Grennberg, H.; Bäckvall, J.-E. *J. Am. Chem. Soc.* **1994**, *116*, 3631.
(26) Arduengo, A. J.; Dias, H. V. R.; Harlow, R. F.; Kline, M. *J. Am. Chem. Soc.* **1992**, *114*, 5530.

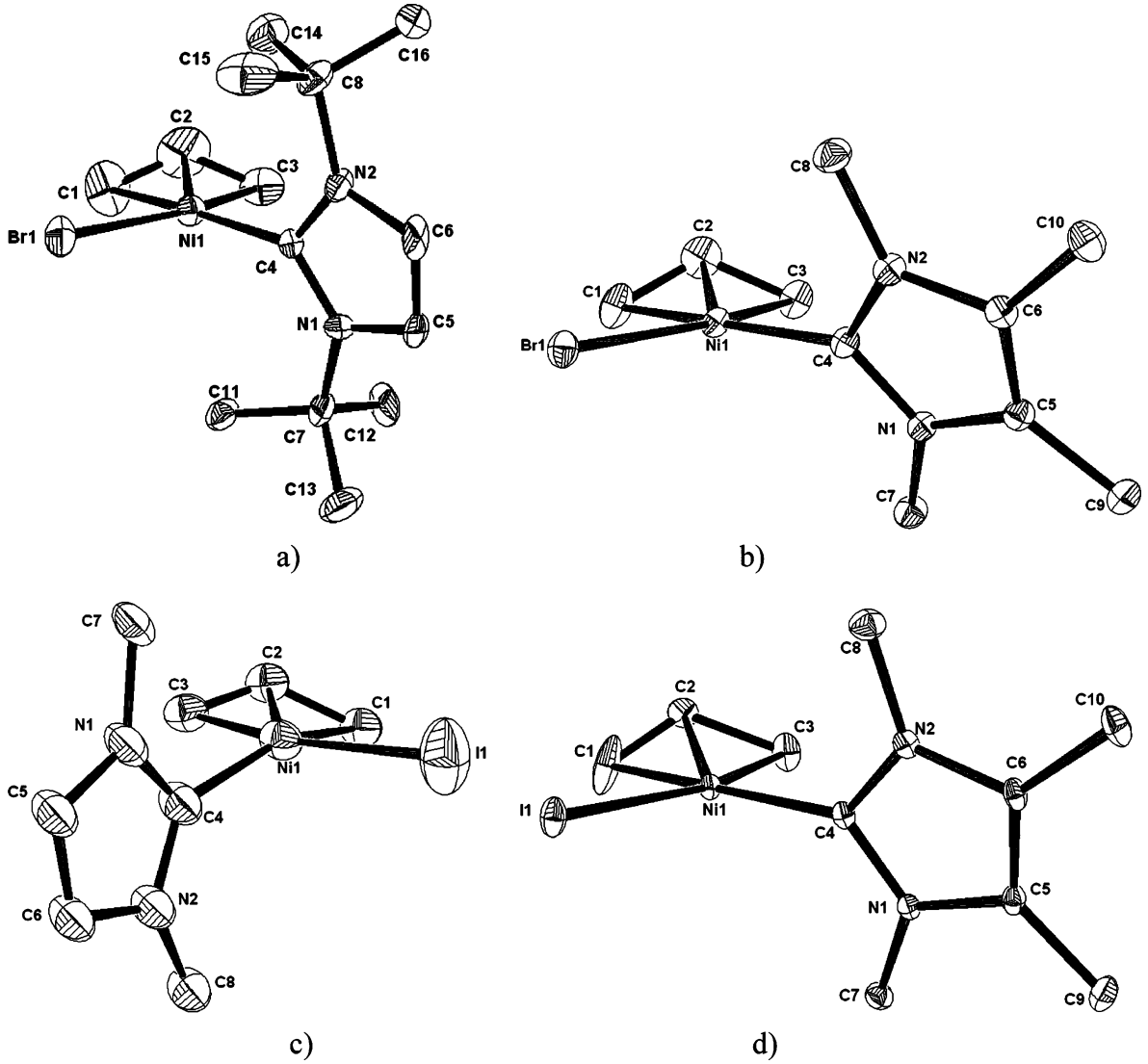

Figure 1. ORTEP III diagrams of compounds (a) **1**, (b) **2**, (c) **4**, and (d) **5** using 25% probability level ellipsoids. Hydrogens were omitted for clarity.

All compounds were obtained as air-sensitive orange-brown crystalline materials and were characterized by elemental analysis and ^{1}H and $^{13}C\{^{1}H\}$ NMR spectroscopy (see Experimental Section).

X-ray Characterization. Compounds were crystallized in cold diethyl ether (**1**), toluene (**2** and **4**), or toluene double-layered with *n*-hexane (**5**), affording crystals that were measured by X-ray diffraction. The four molecular structures are shown in Figure 1. Due to significant disorder over a mirror plane, and at the iodine atom and allyl group, the structure of **4** will not be compared with the others. This structure will be used only as additional analytical evidence for this compound, together with NMR and elemental analysis. In all of the crystal structures, two enantiomers are found in the corresponding unit cell, which are related by a mirror plane.

Selected bond lengths and angles and dihedral angles are given in Table 1, for compounds **1**, **2**, and **5**. Geometries around the nickel atom are essentially square planar, with the halogen atom (Br1 or I1), the NHC carbon atom C4, and the two allyl terminal carbons (C1 and C3) defining the Ni square plane and the related dihedral twist angle A (defined in Table 1) being small (2.9−6.7°). The strong donor ability of imidazol-2-ylidene rings weakens the bond between the metal and the allyl atom placed trans to the carbene ligand (C1). This trans influence results in the increase of Ni1−C1 bond distances compared to those of Ni1−C3 and simultaneous shortening of C1−C2 bonds, which increase their double-bond character in comparison with C2−C3. This asymmetry is reproduced by the DFT results (see below). For complex **5**, particularly short and long distances are found for C1−C2 (1.242(6) Å) and C2−C3 (1.487(4) Å),

Table 1. Selected Bond Lengths (Å), Bond Angles (deg), and Dihedral Angles (deg) for Compounds 1, 2, and 5

	1	**2**	**5**
C1−C2	1.30(2)	1.329(6)	1.242(6)
C2−C3	1.32(2)	1.406(5)	1.487(4)
Ni1−C1	2.058(14)	2.056(3)	2.048(3)
Ni1−C2	1.915(17)	1.984(4)	1.993(3)
Ni1−C3	1.950(14)	1.993(3)	1.982(2)
Ni1−X1	2.372(2)	2.3856(7)	2.5269(9)
Ni1−C4	1.914(13)	1.907(2)	1.9062(18)
C1−C2−C3	130(3)	123.8(4)	123.0(3)
C4−Ni1−X1	97.3(4)	99.09(7)	100.42(7)
dihedral A[a]	6.6	2.9	6.7
dihedral B[b]	63.4	64.8	64.9
dihedral C[c]	82.6	67.4	78.1

[a] Dihedral A: angle between planes (Ni1,X1,C4) and (C1,Ni1,C3). [b] Dihedral B: lowest angle between planes (C1,C2,C3) and (C4,X1,C1,C3,Ni1). [c] Dihedral C: angle between planes (C4,N1,C5,C6,N2) and (C4,X1,C1,C3,Ni1).

Table 2. ^{1}H and ^{13}C NMR Chemical Shifts (δ) of Allyl Nuclei in Compounds 1−5, in C_6D_6, at Room Temperature

	H2^{meso}	H1^{syn}	H1^{anti}	H3^{syn}	H3^{anti}	C2	C1	C3
1	5.01	3.72	2.86	2.32	1.28	105.2	64.5	46.1
2	5.01	3.86	2.86	2.33	1.58	106.8	67.6	44.7
3	4.95	3.85	2.80	2.23	1.47	108.1	67.7	46.0
4	4.80	3.90	2.53	2.57	1.58	106.0	65.5	49.8
5	4.90	3.90	2.59	2.68	1.70	105.9	65.3	49.8

respectively, which are probably due to a certain extent of disorder observed for atom C2 (with 60% and 30% probability).

The bond distances and angles involving the allyl group and the halogens, including the dihedral angle B, between the allyl plane and the Ni square plane (63−65°, with the C2 atom tilting away from the Ni atom), are within the range of those found for complexes of the type [Ni(η^3-allyl)(PR_3)X][27] or for the only structure of the type [Ni(η^3-allyl)(Im)X] (Im = (2,6-^{i}Pr$_2$Ph)$_2$Im; X = Cl) reported in the literature.[20] The distances between the Ni atom and the carbene, Ni1−C4 (1.907−1.914 Å), are very similar to that found for the latter compound (1.903 Å) and are typical of single bonds, such as Ni−Ph bonds (ca. 1.90 Å[28]), in accordance with the reduced π-acceptor character of this class of ligands.[2,29] The Ni1−C4 bond distances are also close to values found for other Ni(II) NHC[30] or diaminocarbene complexes.[31] The dihedral angle C, formed between the NHC ring and the Ni square plane, indicates that the carbene is nearly perpendicular to this plane (82.4°) in compound **1** but is more tilted in compounds **2** (67.4°) and **5** (77.2°). This is attributed to the steric hindrance of the *tert*-butyl groups, which restrain the position of the corresponding NHC ring (see Figure 1a). The NHC *N*-methyl groups in **2** and **5** are not as demanding as the *N*-^{t}Bu in **1** and allow the carbene to tilt in relation to the Ni square plane.

NMR Studies. The NMR spectra of neutral complexes **1**−**5** were assigned on the basis of selective irradiation, DEPT, ^{13}C−^{1}H shift correlations, and nuclear Overhauser effect (NOE) experiments. At this temperature, all these compounds exhibit five distinct and well-defined ^{1}H resonances for the allyl protons, typical of an ABCDX spin pattern, meaning these molecules are asymmetric (C_1 symmetry). Table 2 presents the allyl ^{1}H and ^{13}C resonances for compounds **1**−**5**, in C_6D_6.

The resonances of the allyl terminal protons bound to the carbon atom trans to the NHC ligand, H1^{anti} and H1^{syn}, are always shifted to fields lower than for those corresponding to protons bound to the cis carbon, H3^{anti} and H3^{syn}. The same trend is found in the ^{13}C{^{1}H} NMR spectrum, where the C1 chemical shifts are always higher than those of C3 (Table 2). These shifts are due to a higher degree of localization of the C1−C2 bond as a consequence of the aforementioned trans influence exerted by the NHC ligand.

Scheme 2. Rotation of the NHC Ligand about the Ni−C Bond

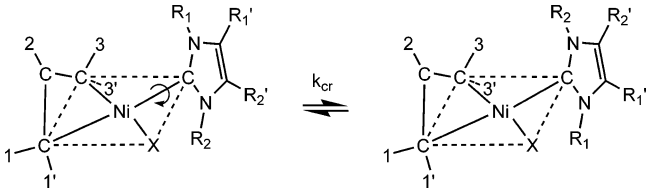

(a) Carbene Rotation. By ^{1}H NMR, the NHC ligand of complex **1** also shows no symmetry: the two ^{t}Bu groups and both protons bound to the carbons of the NHC double bond can be assigned to four different ^{1}H resonances. The variable-temperature (VT) ^{1}H NMR spectra, in toluene-d_8, showed a "static" NHC group, since no detectable line-shape modifications were observed in the range 183−363 K. However, around 313 K, NOE difference experiments showed unambiguous exchange between the ^{t}Bu groups as a result of an extremely hindered rotation about the nickel−carbon bond (Scheme 2). The corresponding $\Delta G^{\ddagger}$ barrier is >18 kcal mol^{-1}. Similar observations were made for the analogous allylpalladium complexes containing ^{t}Bu$_2$Im ligands.[12,19] VT ^{1}H NMR experiments were also performed on solutions of complexes **2**−**5** and indicate that the NHC ligands are fluxional. An example of such experiments is shown in Figure 2, and Table 3 gives the ^{1}H NMR chemical shifts of the carbene ligands of compounds **2**−**5**, in toluene-d_8, measured at temperatures near the slow-exchange limit. At room temperature, the ^{1}H NMR spectrum of the bromine derivative [Ni(η^3-C_3H_5)(Me_4Im)Br] (**2**) shows four fairly broad resonances for the carbene methyl groups, corresponding to a slow rotation of the carbene ligand. A very slow rotation was already detected in the NOE difference spectrum at ca. 263 K. At 299 K, the CCH_3 resonances coalesce into a single peak at δ 1.45 and, as the temperature increases, the NCH_3 resonances become broader and merge at a coalescence temperature (T_C) of 334 K, at ca. δ 3.47. Both resulting resonances sharpen while moving toward the fast-exchange limit, which corresponds to a rapid NHC rotation. Similar observations can be made for [Ni(η^3-C_3H_5)(Me_2Im)Br] (**3**), which, however, shows a much lower NCH_3 coalescence temperature of 295 K (ca. δ 3.4). Conversely, for both iodine derivatives, [Ni(η^3-C_3H_5)(Me_2Im)I] (**4**) and [Ni(η^3-C_3H_5)(Me_4Im)I] (**5**), the ^{1}H NMR spectra show virtually "static" NHC ligands at room temperature, whose rotation is only detected by NOE experiments. Coalescence temperatures of the NCH_3 resonances were obtained respectively at 340 K (δ 3.37) and 366 K (ca. δ 3.5).

The VT ^{1}H NMR spectra allowed the calculation of $\Delta G^{\ddagger}$ values for this process, using complete line-shape analysis.[32] Measurements in solvents other than toluene-d_8 (1,1,2,2-tetrachloroethane-d_2 and bromobenzene-d_5) were also performed for the cases of **3** and **4** and led to values agreeing within ±0.3 kcal mol^{-1}. The results are summarized in Table 4.

According to the "static" NMR features exhibited by compound **1** and the $\Delta G^{\ddagger}$ data shown in Table 4, it is evident that the rotation barrier decreases in the order ^{t}Bu$_2$Im > Me_4Im > Me_2Im and also I > Br. These trends seem to be associated with the steric demand of either the NHC or, to a lesser extent,

(27) (a) Brandes, H.; Goddard, R.; Jolly, P. W.; Kruger, C.; Mynott, R.; Wilke, G. *Z. Naturforsch., B: Chem. Sci.* **1984**, *39*, 1139. (b) Andrews, P.; Corker, J. M.; Evans, J.; Webster, M. *J. Chem. Soc., Dalton Trans.* **1994**, 1337. (c) Cameron, T. S.; Prout, C. K. *Acta Crystallogr., Sect. B: Struct. Crystallogr. Cryst. Chem.* **1972**, *28*, 2021. (d) Belderrain, T. R.; Nicasio, M. C.; Paneque, M.; Poveda, M. L.; Carmona, E. *Gazz. Chim. Ital.* **1994**, *124*, 341. (e) Angermund, K.; Eckerle, A.; Monkiewicz, J.; Kruger, C.; Wilke, G. *Inorg. Chim. Acta* **1998**, *270*, 273.

(28) Bellabarba, R. M.; Gomes, P. T.; Pascu, S. I. *Dalton Trans.* **2003**, 4431.

(29) (a) Green, J. C.; Scurr, R. G.; Arnold, P. L.; Cloke, F. G. N. *Chem. Commun.* **1997**, 1963. (b) Zheng, X.; Herberich, G. E. *Organometallics* **2000**, *19*, 3751.

(30) For example: (a) Herrmann, W. A.; Gerstberger, G.; Spiegler, M. *Organometallics* **1997**, *16*, 2209. (b) Abernethy, C. D.; Clyburne, J. A. C.; Cowley, A. H.; Jones, R. A. *J. Am. Chem. Soc.* **1999**, *121*, 2329. (c) Douthwaite, R. E.; Haüssinger, D.; Green, M. L. H.; Silcock, P. J.; Gomes, P. T.; Martins, A. M.; Danopoulos, A. A. *Organometallics* **1999**, *18*, 4584. (d) Abernethy, C. D.; Cowley, A. H.; Jones, R. A. *J. Organomet. Chem.* **2000**, *596*, 3. (e) Douthwaite, R. E.; Green, M. L. H.; Silcock, P. J.; Gomes, P. T. *Organometallics* **2001**, *20*, 2611. (f) Sun, H. M.; Shao, Q.; Hu, D. M.; Li, W. F.; Shen, Q.; Zhang, Y. *Organometallics* **2005**, *24*, 331.

(31) Kremzow, D.; Seidel, G.; Lehmann, C. W.; Fürstner, A. *Chem. Eur. J.* **2005**, *11*, 1833.

(32) Friebolin, H. *Basic One- and Two-Dimensional NMR Spectroscopy*; VCH: New York, 1991; Chapter 11.

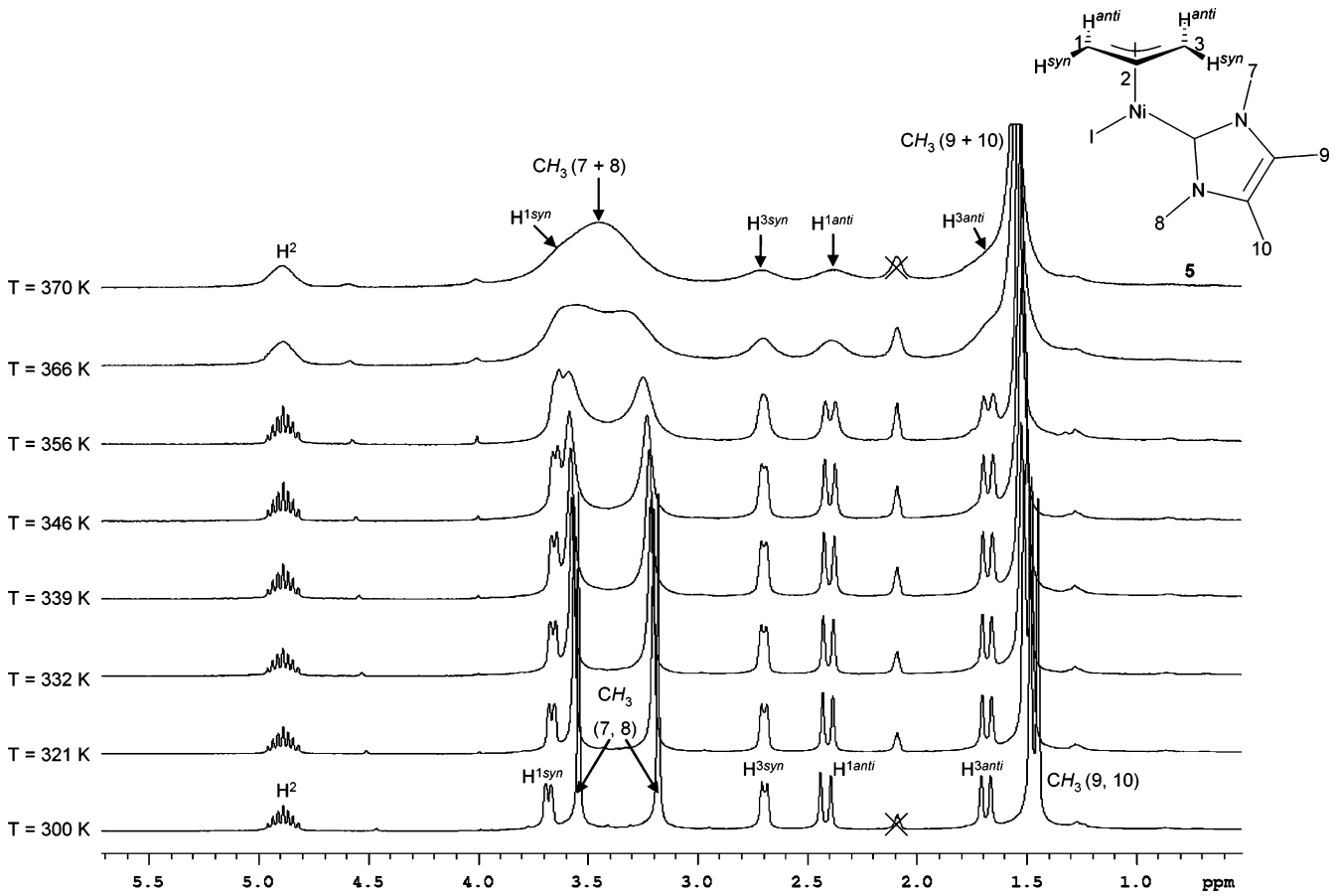

Figure 2. VT ^{1}H NMR experiments for compound **5**, in toluene-d_8.

Table 3. ^{1}H NMR Chemical Shifts (δ) of "Static" NHC Nuclei in Compounds 2−5, in Toluene-d_8

	T (K)	NCH_3 (7)	NCH_3 (8)	CCH_3 (9)	CCH_3 (10)	C*H* (5)	C*H* (6)
2	215	3.12	3.57	1.32	1.34		
3	215	3.03	3.47			5.76	5.82
4	room temp[a]	3.14	3.49			6.01	6.07
5	room temp[a]	3.17	3.54	1.44	1.47		

[a] Room temperature (ca. 295 K).

Table 4. $\Delta G^{\ddagger}$ Values for Carbene Rotation in Compounds 2−5, at 298 K, and Corresponding Rate Constants, Calculated from the NCH_3 ^{1}H NMR Resonances

			k_{cr} (s^{-1})		
complex	solvent	T_C (K)	298 K	T_C	$\Delta G^{\ddagger}_{298}$[a] (kcal mol^{-1})
2	toluene-d_8	334	18	290	15.8
3	toluene-d_8	295	363	314	14.0
	$CDCl_2CDCl_2$	306	170	264	14.6
	toluene-d_8	340	17	184	15.8
4	$CDCl_2CDCl_2$	343	11	238	16.0
	C_6D_5Br	326	37	172	15.4
5	toluene-d_8	366	0.6	183	17.8

[a] ±0.7 kcal mol^{-1}.

the halide ligands, as indicated by the DFT results (see below). In fact, the ^{t}Bu$_2$Im is locked in its coordination position by the volume of the ^{t}Bu substituents, whereas the less bulky Me groups confer to these ligands a higher degree of rotational freedom. It has been often pointed out that the metal−NHC rotation barrier is only steric in nature and is not influenced by electronic factors, since the metal−carbene bond has essentially single-bond character due to the nonexistent π-back-bonding.[6,17,22] Although steric constraints imposed by Me$_2$Im or Me$_4$Im are basically the same, rotation barriers are slightly higher for the Me$_4$Im derivatives. This aspect is studied below using DFT calculations.

(b) Allyl Rotation. It is well-known that allylnickel complexes may undergo isomerization processes.[21a,23] X-ray structures of **1**, **2**, and **5** had already shown that two enantiomers are present in the solid state in the ratio 1:1. Although they certainly coexist in solution, the two isoenergetic isomers, related by a mirror plane perpendicular to the Ni square plane, are indistinguishable by NMR. To determine whether these isomers take part in interconversion equilibria and assess the possible mechanisms involved, variable-temperature NOE difference experiments were performed. At very low temperatures, for compounds **1**−**5**, no exchange between the allyl resonances is detected by NOE, ruling out interconversion between the isomers. However, as the temperature increases (above 333 K for **1** and below room temperature for the others), slow exchange between the two anti-hydrogen resonances and also between the two syn-hydrogen resonances are observed: syn−syn, anti−anti exchange. This second fluxional process observed in these molecules is also called cis−trans isomerization and may be interpreted in two ways: (a) rotation of the allyl ligand, in its own plane, about the Ni−η^3-allyl axis (or an angular twist of ligands NHC and X, Scheme 3) and (b) reorganization of the entire complex accomplished by pseudorotation of all ligands. Process b, usually called *apparent allyl rotation*, can involve dissociative (dissociation of NHC or X ligands) or associative pathways (coordination of solvent or other donor molecules present in the solution). The first case (pure allyl rotation, process a) was described for [Ni(η^3-allyl)(L)R] (L = phosphine;

Scheme 3. Rotation of the Allyl Ligand, in Its Own Plane, about the Ni−η^3-allyl Axis (Syn−Syn, Anti−Anti Exchange)

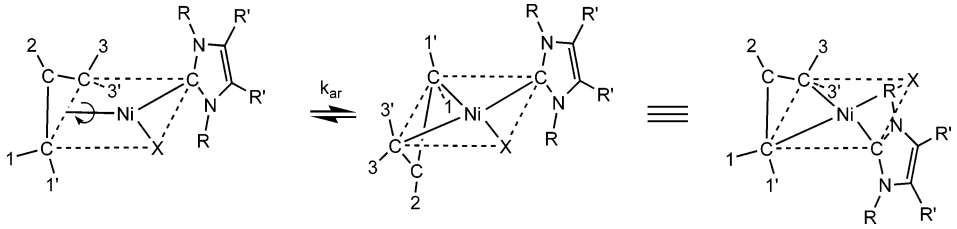

Table 5. Activation Parameters for the Allyl Anti-Hydrogen Exchange (Allyl Rotation) in Complex 4, in Bromobenzene-d_5

$\Delta H^{\ddagger}$ (kcal mol^{-1})	18.0 ± 0.7
$\Delta S^{\ddagger}$ (cal mol^{-1} K^{-1})	5.4 ± 2.2
$\Delta G^{\ddagger}_{298}$ (kcal mol^{-1})	16.4 ± 1.4
k_{ar} (s^{-1})	6;[a] 236[b]

[a] At 298 K. [b] At $T_C = 337$ K.

R = H, Me),[21a] and other non group 10 allyl complexes.[23,33] The second case (apparent allyl rotation, process b) is associated with isomerization in allyl complexes such as [Ni(η^3-allyl)-(NH_2R)CH_3],[21a] [Ni(η^3-allyl)(PPh_3)X],[21a] and [Pd(η^3-C_4H_7)(L)-Cl] (L = $AsPh_3$, PPh_3, CO)[23] and also with allyl Pd complexes containing bidentate nitrogen ligands,[24,25,34−38] where isomerizations result from bimolecular reactions with other molecules. In most cases both mechanisms can be considered.

In the range of temperatures studied, the VT ^{1}H NMR spectra obtained for compounds **2**−**5**, in either toluene-d_8 or 1,1,2,2-tetrachloroethane-d_2, show some broadening of allyl proton resonances, though it is insufficient to reach a coalescence temperature. However, the use of bromobenzene-d_5 seems to accelerate the exchange process for complex **4** and enabled the observation of coalescence of the terminal allyl proton resonances at ca. 337 K, decomposition being detected readily above this temperature. This observation allowed the determination of an experimental value of $\Delta H^{\ddagger}$ for compound **4**, employing complete line-shape analysis for the anti-hydrogen resonances. The activation parameters for this process were calculated from the corresponding Eyring plot and their values are given in Table 5.

An experimental $\Delta H^{\ddagger} = 18$ kcal mol^{-1} is obtained for the allyl rotation process. A value of 16.4 kcal mol^{-1} is determined for the corresponding Gibbs activation energy, at 298 K, which is close to the $\Delta G^{\ddagger}$ values determined for the π-allyl rotation observed in the complexes [Mo(η^3-C_3H_5)(CO)(L_2)(dppm)] when $L_2 = S_2CNC_4H_8$ (15.6 kcal mol^{-1}), S_2CNEt_2 (14.7 kcal mol^{-1}), in $CDCl_3$.[33] No coalescence is observed up to 373 K in toluene-d_8 solutions of complex **4**. The exact $\Delta G^{\ddagger}$ value cannot be determined, corresponding though to a rotation barrier of $\Delta G^{\ddagger} > 17$ kcal mol^{-1}.

It is also clear that cis−trans isomerization is unfavorable in compound **1** in comparison to the case for the other complexes **2**−**5**, because syn−syn, anti−anti exchange occurs at much higher temperatures in the first case. This agrees with a more hindered rotation of the allyl ligand in **1** due to the bulkiness of the NHC *tert*-butyl groups.

DFT calculations indicate that pure rotation of the allyl ligand about the Ni−η^3-allyl axis is possible through a "spin-forbidden" path involving spin singlet and spin triplet species (see below), which may explain the syn−syn, anti−anti exchange observed experimentally.

(c) Allyl η^3−η^1−η^3 Isomerization. When the temperature is increased further, a third fluxional process is detected. Around 353 K, for compound **1**, saturation transfer is selectively observed between the geminal syn and anti hydrogens bound to the terminal allyl carbon cis to the NHC ligand (C3):syn−anti exchange. For complexes **2**−**5**, at temperatures in the range 323−353 K, all terminal allyl protons exchange between them, in most cases with simultaneous resonances broadening. When toluene-d_8 is used as the solvent, these processes are reversible, without significant decomposition. However, if 1,1,2,2-tetrachloroethane-d_2 is used instead, compound **3** decomposes immediately after syn−anti exchange is detected (ca. 343 K). When the solvent is bromobenzene-d_5, complex **4** decomposes above 337 K, after coalescence of the terminal allyl proton resonances is observed.

The anti−syn exchange occurring at high temperatures is commonly detected in allyl complexes, either restricted to one side of the allyl ligand (as observed for compound **1**, above 353 K) or occurring at both sides (as detected for compounds **2**−**5** at lower temperatures). This exchange is associated with an allyl η^3−η^1−η^3 isomerization,[23,37,39−42] as is illustrated in Scheme 4.

Studies of several allylruthenium complexes with a variety of ligands with different electron-donating strengths allowed the conclusion that strong σ-donor ligands favor the η^3−η^1−η^3 process.[23] The first step is the destabilization of the initial π-allyl state, promoted by strong trans effects induced by very basic ligands,[23] such as those imidazol-2-ylidenes employed in this work. The same mechanism was proposed to explain the coalescence of the resonances corresponding to protons 3 and 3′ in the complex [Pd(η^3-2-CH_3-C_3H_4)(L)Cl], with L being $PPhMe_2$ or PPh_3.[23] Despite this, there is some evidence that the π−σ−π mechanism may be controlled by steric and not electronic effects.[42]

We believe that the terminal carbon trans to the NHC ligand (with the largest trans influence/effect) leaves the nickel atom, resulting in a σ-allyl species (Scheme 4). In fact, a detailed DFT mechanism for this step is discussed below (see Molecular Orbital Calculations), which points to a rearrangement of the

(33) Yih, K.-H.; Lee, G.-H.; Huang, S.-L.; Wang, Y. *Organometallics* **2002**, *21*, 5767.
(34) Crociani, B.; Antonaroli, S.; Paci, M. *Organometallics* **1997**, *16*, 384.
(35) Guerrero, A.; Jalón, F. A.; Manzano, B. R.; Rodríguez, A.; Claramunt, R. M.; Cornago, P.; Milata, V.; Elguero, J. *Eur. J. Inorg. Chem.* **2004**, 549.
(36) Takao, Y.; Takeda, T. *Organometallics* **1999**, *18*, 2936.
(37) Carrión, M. C.; Díaz, A.; Guerrero, A.; Jalón, F. A.; Manzano, B. R.; Rodríguez, A.; Paul, R. L.; Jeffrey, J. C. *J. Organomet. Chem.* **2002**, *650*, 210.
(38) Torre, F. G.; Hoz, A.; Jalón, F. A.; Manzano, B. R.; Rodríguez, A. M. *Inorg. Chem.* **2000**, *39*, 1152.
(39) Solin, N.; Szabó, K. J. *Organometallics* **2001**, *20*, 5464.
(40) Schwarz, I.; Rust, J.; Lehmann, C. W.; Braun, M. *J. Organomet. Chem.* **2000**, *605*, 109.
(41) Henc, B.; Jolly, P. W.; Salz, R.; Stobbe, S.; Wilke, G.; Benn, R.; Mynott, R.; Seevogel, K.; Goddard, R.; Krüger, C. *J. Organomet. Chem.* **1980**, *191*, 449.
(42) Pregosin, P. S.; Salzmann, R.; Togni, A. *Organometallics* **1995**, *14*, 842.

Scheme 4. Allyl $\eta^3-\eta^1-\eta^3$ Isomerization (Syn−Anti Exchange)

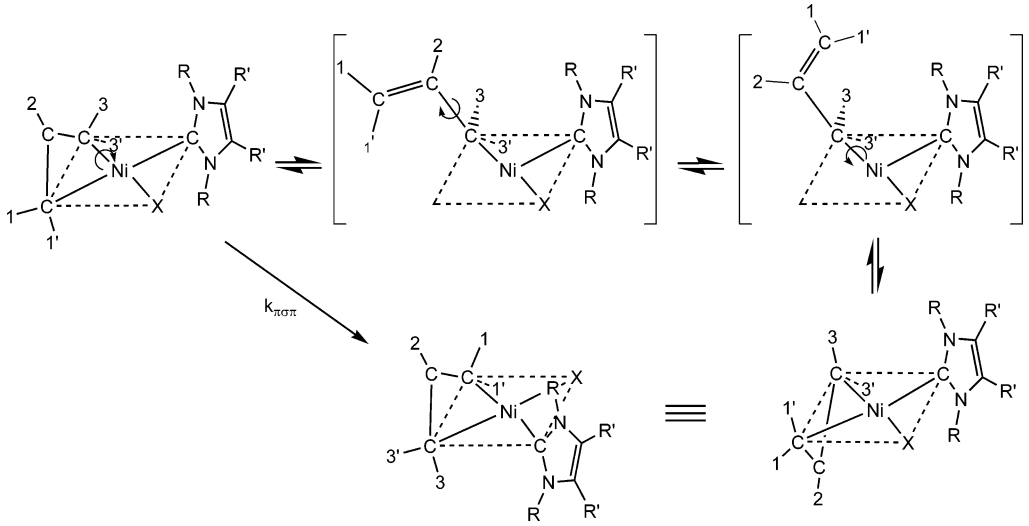

Scheme 5. Exchange Pathways Observed in Compounds (a) 1 ($k_{ar} \approx k_{\pi\sigma\pi}$) and (b) 2−5 ($k_{ar} > k_{\pi\sigma\pi}$) at High Temperatures

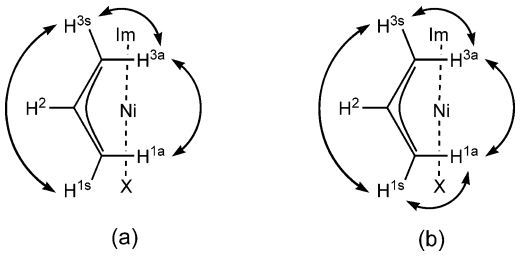

ligands in the Ni square plane, leading to a T-shaped intermediate slightly different from that depicted in Scheme 4. The protons 3 and 3′ (cis to the carbene) interchange through a simple rotation around the allyl C3(sp^3)−C2(sp^2) bond (Schemes 4 and 5a), and subsequent rotation about Ni−C3 bond regenerates the η^3 coordination of the allyl ligand.[23,43]

The simultaneous occurrence of a faster allyl rotation in its own plane could explain the additional exchange observed between terminal protons 1 and 1′, in compounds **2**−**5** (Scheme 5b) and corresponds to the situation where the allyl rotation rate constant, k_{ar}, is higher than the $\eta^3-\eta^1-\eta^3$ isomerization rate constant, $k_{\pi\sigma\pi}$ (i.e. $k_{ar} > k_{\pi\sigma\pi}$). In fact, due to a fast allyl rotation, *both* terminal allyl carbons "see", in average, the carbene ligand in the trans position, being both equally destabilized by the trans effect exerted by this basic ligand.

In compound **1**, the allyl rotation occurs slower than in compounds **2**−**5** and a selective syn−anti exchange restricted to 3 and 3′ (Scheme 5a) is observed above 353 K. This may be explained by a decrease of the allyl rotation rate constant (k_{ar}) to values near those of the $\eta^3-\eta^1-\eta^3$ isomerization rate constant ($k_{ar} \approx k_{\pi\sigma\pi}$). In this case, the net result will be that, in practice, only one of the allyl terminal carbons (C1) will be trans to the carbene ligand.

In summary, we observed three different exchange processes occurring simultaneously in solutions of compounds **1**−**5**: (a) rotation of the NHC ligand about the Ni−carbon bond, (b) at moderate temperatures, allyl rotation about the Ni−allyl axis, resulting in syn−syn, anti−anti exchange, and (c) at high temperatures, allyl $\eta^3-\eta^1-\eta^3$ isomerization, resulting in syn−anti exchange.

Molecular Orbital Calculations. DFT calculations[44] were performed in order to rationalize the fluxional behavior experimentally observed for the allyl and the carbene (NHC) ligands of complexes [Ni(η^3-C_3H_5)(Im)X]. The influence of both the halogen and the carbene ligands was studied by means of calculations on molecules with Im = Me_4Im (X = Br (**2**)) and with Im = Me_2Im (X = Cl (**6**), Br (**3**), I (**4**)).

The geometries optimized for all species correspond to square-planar complexes and are, in general, in very good agreement with the X-ray structures discussed above. For example, for complex **2**, the maximum and mean absolute deviation between experimental (from synchrotron X-ray diffraction data) and optimized Ni−X bond distances are 0.065 and 0.030 Å, respectively. In particular, the coordination asymmetry of the allyl ligand is clearly reproduced by the calculations. Also for **2**, the Ni−C3[45] distance (2.024 Å) is shorter than that corresponding to Ni−C1 (2.104 Å), and C1−C2 (1.394 Å) is shorter than C2−C3 (1.420 Å). Those differences become clearer when electronic factors are considered. The corresponding Wiberg indices (WI), well-known bond strength indicators,[46] are 0.423, 0.339, 1.506, and 1.362, respectively, showing that shorter distances correspond, indeed, to stronger bonds.

NMR data indicate that carbene rotation around the Ni−C4 axis is the more facile fluxional process for complexes of the type [Ni(η^3-C_3H_5)(Im)X]. Figure 3 shows the corresponding free energy profiles calculated for complexes **2**−**4** and **6**. As rotation occurs, the carbene conformation relative to the plane of the complex moves from clearly tilted in the minima to practically coplanar in the transition state (**TSC**),[47] while the square-planar arrangement around the metal is maintained along the process. The values calculated for $\Delta G^{\ddagger}$ are in good agreement (within

(43) Herrmann, J.; Pregosin, P. S.; Salzmann, R. *Organometallics* **1995**, *14*, 3311.

(44) Parr, R. G.; Yang, W. *Density Functional Theory of Atoms and Molecules*; Oxford University Press: New York, 1989.

(45) The labeling scheme used in the X-ray structures (Figure 1) is maintained in the text.

(46) (a) Wiberg, K. B. *Tetrahedron* **1968**, *24*, 1083. (b) Wiberg indices are electronic parameters related to the electron density between atoms. They can be obtained from a natural population analysis and provide an indication of the bond strength.

(47) The tilting of the carbene ligand is given by the dihedral angle C, measured between the mean plane of the five-membered-ring carbene and the mean Ni square plane (see Table 1). For the optimized geometries of the complexes with Im = Me_2Im, that angle varies from 71 (**6**), 73 (**3**), and 84°(**4**), in the minima, to 7° in the three transition states (**TSC**). In the case of complex **2**, the tilt angle varies from 85° in the minimum to 3° in the transition state.

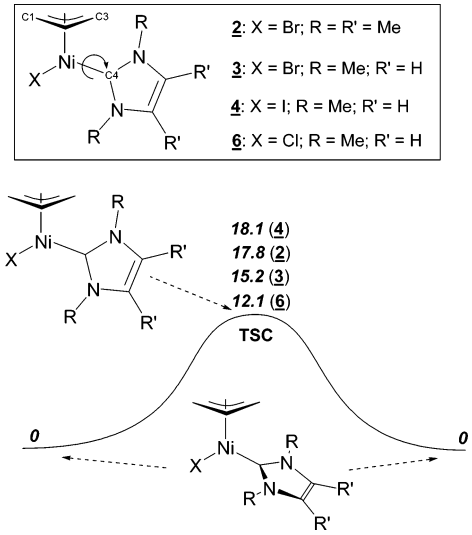

Figure 3. General free energy profile (values given in italics, in kcal mol^{-1}) calculated for the NHC rotation around the Ni−C bond, in [Ni(η^3-C_3H_5)(Im)X] complexes.

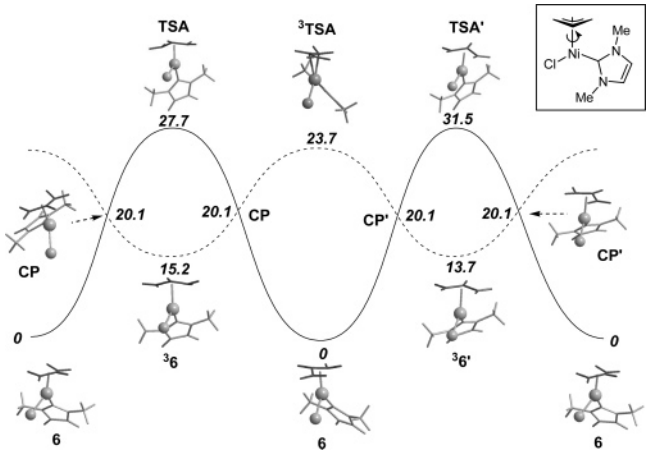

Figure 4. Energy profile calculated for the allyl rotation in [Ni(η^3-C_3H_5)(Me_2Im)Cl]. The relevant points were optimized (B3LYP) and the corresponding structures are presented. The energies (in italics, in kcal mol^{-1}) are referenced to the most stable species, complex **6**. The plain curve corresponds to the spin singlet ($S = 0$) PES and the dashed curve to the spin triplet ($S = 1$) PES.

2.3 kcal mol^{-1}) with those experimentally determined for **2**−**4** (see Table 4).

The trend corresponding to higher activation energies for NHC rotation as X descends within the halogen group is clearly reproduced by the calculations for the entire series of complexes with Im = Me_2Im, including the species with X = Cl. This is related to the steric bulkiness of the halogen ligand, as previously suggested in the discussion of the NMR results (see above), and can be assigned to the geometrical distortion suffered by the molecules during the rotation. In fact, carbene rotation brings the methyl substituents on the nitrogen atoms into close proximity of the halogen, especially in the transition state. The geometrical distortion of the square-planar geometry around the metal, as the rotation proceeds, can be evaluated by the variation of the X−Ni−C4 angle along the process. This angle is 95° for complexes **3**, **4**, and **6**, with a maximum 0.3° difference in the three molecules. As rotation occurs and the transition is reached, that angle opens up to 103, 106, and 108°, respectively, for X = Cl, Br, I, demonstrating that the degree of distortion increases with the size of the halogen ligand.

Carbene rotation depends also on the nature of the NHC ligand, even when the difference lies only on the outer side of this ligand, that is on the C=C substituents: H in the case of complex **3** and methyl for complex **2**. Rotation is more difficult in the complex containing the tetramethyl-substituted Me_4Im carbene, and the experimental $\Delta G^{\ddagger}$ difference between **2** and **3** (2 kcal mol^{-1}) is well reproduced by the calculations (2.6 kcal mol^{-1}). Although the differences between the transition states (**TSC**) optimized for the two species **2** and **3** are very subtle, a more distorted geometry exists in the case of **TSC(2)** (Br−Ni−C4 = 107.1°), as compared to that in **TSC(3)** (Br−Ni −C4 = 105.8°). In addition, the Ni−Br bond is longer (2.450 Å) and weaker (WI = 0.356) in **TSC(2)** than in **TSC(3)** (d_{Ni-Br} = 2.434 Å, WI = 0.363). The same trend is observed for the Ni−C(carbene) distance: d_{Ni-C4} = 2.016 Å, WI = 0.444 for **TSC-(2)** and d_{Ni-C4} = 2.000 Å, WI = 0.449 for **TSC(3)**. Weaker bonds in **TSC(2)** result in a electron poorer metal, as shown by the corresponding charge, obtained from a natural population analysis (NPA):[48] 0.59 in **TSC(2)** and 0.58 in **TSC(3)**. Although the differences are very small and, as such, any conclusion should be taken with caution, the results indicate that a slightly more severe distortion of the square-planar geometry is needed during the carbene rotation in the case of **2**, justifying the difference observed in the activation parameters. Therefore, the difference observed between experimental $\Delta G^{\ddagger}$ values of **2** and **3** may be attributed basically to steric effects existing mainly in the transition states.

A fluxional process corresponding to allyl rotation around the Ni−(η^3-allyl) axis is indicated by NMR (see above). However, the mechanism followed by such a process cannot be established, solely on the basis of the experimental results. The data may fit a simple intramolecular path, or alternatively, a more complex mechanism, involving ligand association or dissociation, may be at work. The intramolecular path was investigated by means of DFT calculations in order to test whether such a mechanism may be responsible for the observed fluxionality. Given the excellent performance of the theoretical method in the description of the carbene rotation for all molecules addressed, the study was performed on the species having the simplest carbene ligand (Me_2Im) and the smallest halogen (Cl), [Ni(η^3-C_3H_5)(Me_2Im)Cl] (**6**), to have the best possible compromise between computational time and accuracy of the results.

The energy profile calculated for the rotation of the allyl in complex **6** is depicted in Figure 4. In **6**, a 180° rotation of the allyl group completes the process of isomerization. This corresponds to a symmetrical profile, since the allyl ends up in a conformation equivalent to the starting one (enantiomeric, in fact): a formally Ni(II) square-planar complex with two coordination positions occupied by the allyl terminal carbons, another by Cl, and the last one by the NHC ligand. However, given the presence of two different coligands, two distinct directions exist for the allyl rotation movement. In one case the allyl meso carbon (C2) passes over the Cl atom, while the other brings the allyl C2 over the carbene ligand. The two

(48) (a) Carpenter, J. E.; Weinhold, F. *J. Mol. Struct. (THEOCHEM)* **1988**, *169*, 41. (b) Carpenter, J. E. Ph.D. Thesis, University of Wisconsin, Madison, WI, 1987. (c) Foster, J. P.; Weinhold, F. *J. Am. Chem. Soc.* **1980**, *102*, 7211. (d) Reed, A. E.; Weinhold, F. *J. Chem. Phys.* **1983**, *78*, 4066. (e) Reed, A. E.; Weinhold, F. *J. Chem. Phys.* **1983**, *78*, 1736. (f) Reed, A. E.; Weinstock, R. B.; Weinhold, F. *J. Chem. Phys.* **1985**, *83*, 735. (g) Reed, A. E.; Curtiss, L. A.; Weinhold, F. *Chem. Rev.* **1988**, *88*, 899. (h) Weinhold, F.; Carpenter, J. E. *The Structure of Small Molecules and Ions*; Plenum: New York, 1988; p 227.

transition states optimized for those processes, respectively, **TSA** and **TSA′**, describe the allyl rotation along the spin singlet potential energy surface (PES). This is the most stable spin state of the initial complex, **6**, as expected for a square-planar d^8 complex. The activation energies obtained indicate that rotation over Cl, i.e., going through **TSA**, is more facile ($\Delta E^{\ddagger} = 27.1$ kcal mol^{-1}) than that going over the carbene (**TSA′**, $\Delta E^{\ddagger} =$ 31.5 kcal mol^{-1}), due to the bulkiness of the *N*-methyl substituents. The values calculated for the activation energy of the allyl rotation are too high, in comparison to the experimental activation enthalpy determined for complex **4** (18.0 kcal mol^{-1}). At first sight, this could suggest that the allyl fluxionality would follow a different mechanism. However, a deeper analysis of the results shows that an important factor was disregarded. In fact, both structures of the transition states **TSA** and **TSA′** (Figure 4) correspond to ca. 90° rotations of the allyl ligand about the Ni−allyl bond, starting from the structure of compound **6**. While reactant **6** is formally a square-planar complex, the two transition states, **TSA** and **TSA′**, correspond, in fact, to *tetrahedral* complexes. This can be quantified by the dihedral angle C between the Ni(allyl) plane (defined by Ni, C1, and C3) and the Ni(carbene)Cl plane (defined by Ni, C4, and Cl), which measure 1° in structure **6** and 88 and 89° in **TSA** and **TSA′**, respectively. These angles are very close to the ideal values for square-planar complexes (0°), in the case of **6**, or tetrahedral species (90°), for the transition states. Now, if a spin singlet is what one should expect for a d^8 square-planar complex, a spin triplet is the preferential state of a tetrahedral species with the same electron count.[49]

The energy profile calculated for the complete rotation of the allyl ligand along the spin triplet PES is represented with a dashed line in Figure 4. Naturally, the relative conformation of the two planes, Ni(allyl) and Ni(carbene)Cl, in the minima of this profile (^{3}**6** and ^{3}**6′**) are equivalent to those existing in the transition states of the $S = 0$ PES, **TSA** and **TSA′** (*S* being the total spin of the molecule). Conversely, the same relative conformation is observed between the minimum of the singlet surface (**6**) and the transition state of the triplet (^{3}**TSA**). In other words, the former correspond to tetrahedral species, while the latter are square-planar molecules. The superscript in the labels of the relevant points along the $S = 1$ PES correspond to the spin multiplicity ($2S + 1$).

Two interesting conclusions arise from the comparison of the singlet and the triplet energy profiles, in Figure 4. The first is that the spin singlet square-planar complex **6** is the most stable of all species. This is what is expected for a d^8 metal complex with a coordination number of 4, as mentioned above. The second conclusion is that allyl rotation is considerably more facile in the triplet PES ($\Delta E^{\ddagger} = 8.5$ and 10.0 kcal mol^{-1}) than in the singlet surface. Both results are due to the same reason. For a d^8 electron count, high-spin compounds have greater occupation of M−L antibonding orbitals than a low-spin square-planar species.[49] This accounts not only for the relative stability of the minima but also for the rotation energy barrier. In fact, an increased occupation of antibonding orbitals results in longer metal−ligand distances and, thus, in less crowded transition states for the allyl rotation. For example, when the square-planar species **6** and ^{3}**TSA** are compared, the mean Ni−C(allyl) distance is 2.06 Å in **6** and 2.56 Å in ^{3}**TSA**; the same trend is verified for the Ni−Cl bond (2.232 Å in **6**, and 2.258 Å in ^{3}**TSA**) and for the Ni−C(carbene) distance (1.918 Å in **6**, and 2.048 Å in ^{3}**TSA**).

For certain geometries of the [Ni(η^3-C_3H_5)(Me_2Im)Cl] species, intermediate between square-planar and tetrahedral, the two PES in Figure 4 approach and, eventually, may cross each other. Should allyl rotation involve the participation of both PES, than it would correspond to a "spin-forbidden" or "nonadiabatic" process with a change in the spin state, starting with a singlet reactant (**6**), going through a triplet intermediate (^{3}**6** or ^{3}**6′**), and ending up in a singlet product (**6**). The energy profiles of those processes go through minimum energy crossing points (MECP) corresponding to the lowest energy points at which the energy and the geometry of the molecule are the same in the two surfaces: in this case the spin singlet and the spin triplet surfaces. Once the MECP is reached, the system has a given probability of changing its spin state and, thus, hops from one surface to the other, completing the reaction.[50]

Two MECP could be optimized for the allyl rotation process: one for the rotation over Cl, connecting **6** with ^{3}**6** (**CP**) and the other corresponding to the rotation over the carbene ligand, involving ^{3}**6′** as the intermediate (**CP′**). The geometrical arrangement around the metal in the MECP is between tetrahedral and square planar, as shown by the dihedral angle C between the Ni(allyl) and the Ni(carbene)Cl planes: 61° for **CP** and 53° for **CP′**. From the complete profile of Figure 4 (MECP included) the most favorable path calculated for the rotation of the allyl ligand over the Cl is **6** → **CP** → ^{3}**6** → **CP** → **6**, while the rotation in the other direction, that is, over the carbene, corresponds to **6** → **CP′** → ^{3}**6′** → **CP′** → **6**. These are two-step mechanisms involving spin triplet tetrahedral species (^{3}**6** and ^{3}**6′**) as reactive intermediates. The rate-limiting step corresponds to the first one, in both cases, i.e., the conversion of the square-planar singlet into the tetrahedral triplet, and the activation energy calculated for those processes ($\Delta E^{\ddagger} = 20.1$ kcal mol^{-1}) is in very good agreement with the experimental activation enthalpy (18.0 kcal mol^{-1}, see above), thus providing a strong indication that allyl rotation may proceed via this intramolecular "nonadiabatic" path involving spin singlet and spin triplet species. The absence of experimental detection of paramagnetism due to spin triplet intermediates should be attributed to the short-lived nature of this species, as corroborated by the small energy barrier associated with the regeneration of **6** from those intermediates: 4.9 (^{3}**6**) and 6.3 kcal mol^{-1} (^{3}**6′**).

In principle, this type of spin crossover mechanism can operate in similar dynamic processes occurring in [Ni(η^3-allyl)-LX] square-planar complexes. However, the nature of L and X ligands will play a crucial role in the spin state splitting energy, and, consequently, in the energy difference between the spin singlet and triplet PES. For example, better donor ligands are expected to stabilize the $S = 0$ square-planar species with respect to the $S = 1$ tetrahedral complex, thus making the spin crossover mechanism less likely to occur in comparison with other possible alternatives, such as associative (e.g. solvent-assisted) or dissociative mechanisms involving allyl $\eta^3-\eta^1$ shifts.

The third fluxional process detected experimentally (allyl $\eta^3-\eta^1-\eta^3$ isomerization) was also studied by means of DFT calculations. The free energy profile for the $\eta^3-\eta^1$ shift of the allyl ligand in **6** is represented in Figure 5, as well as the rotation around the allyl C3−C2 bond in the η^1-allyl species **7** and **7′**.

The first step (Figure 5, left) represents the shift of the allyl ligand from η^3 coordination, in the square-planar reactant **6**, to

(49) Albright, T. A.; Burdett, J. K.; Whangbo, M. H. *Orbital Interactions in Chemistry*; Wiley: New York, 1985; p 295.

(50) For excellent reviews on MECP and their location for transition-metal complexes, see: (a) Harvey, J. N.; Poli, R.; Smith, K. M. *Coord. Chem. Rev.* **2003**, *238−239*, 347. (b) Poli, R.; Harvey, J. N. *Chem. Soc. Rev.* **2003**, *32*, 1.

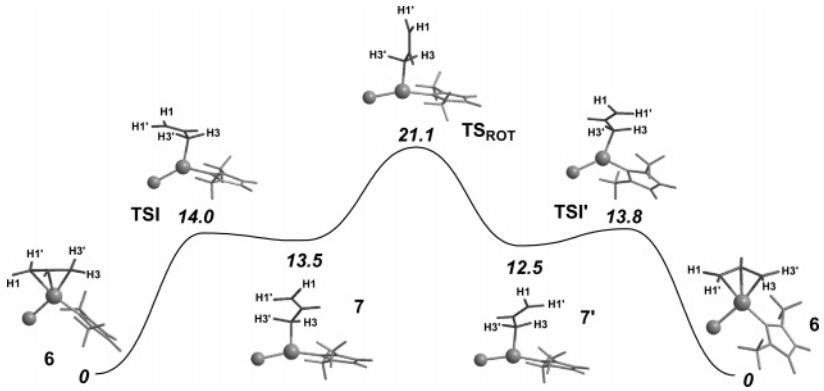

Figure 5. Free energy profile (italics in kcal mol^{-1}) for the allyl $\eta^3-\eta^1-\eta^3$ isomerization in [Ni(η^3-C_3H_5)(Me_2Im)Cl] (**6**) and rotation of the C3(sp^3)−C2(sp^2) bond in the η^1-allyl T-shaped intermediates. The relevant points were optimized (B3LYP), and the corresponding structures are presented.

a η^1 mode in the intermediate [Ni(η^1-allyl)(Me_2Im)Cl] (**7**), a species with a coordination number of 3 and a T-shaped geometry. The process occurs through the breaking of the Ni−C1 bond, which is the carbon trans to the carbene ligand in **6**, corresponding to the weaker Ni−C terminal allyl bond (see above). This distance increses from 2.23 Å in **6** to 3.62 Å in **7**. The coordination position occupied by C1 in **6** is taken by the chloride ligand in intermediate **7**, and the major geometric change along the reaction, besides the breaking of Ni−C1, is the opening of the Cl−Ni−Im angle from 95° in **6** to 161° in **7**. This reaction presents a late transition state (**TSI**), with a wide Cl−Ni−Im angle (138°) and the cleavage of the Ni−C1 bond practically accomplished (d_{Ni-C1} = 3.41 Å, WI_{Ni-C1} = 0.100). This $\eta^3-\eta^1$ shift of the allyl ligand is an endoenergetic process (ΔG = 13.5 kcal mol^{-1}), which means that the T-shaped intermediate is a rather unstable species, but the activation free energy involved ($\Delta G^{\ddagger}$ = 14.0 kcal mol^{-1}) is quite accessible.

From **7**, a rotation around the C3(sp^3)−C2(sp^2) bond of the allyl ligand gives the other T-shaped η^1-allyl intermediate, **7′**, with a different configuration of the allyl ligand, corresponding to the middle step in Figure 5. While in **7** the allyl meso carbon (C2) is facing the carbene, in **7′** this same atom is on the chloride ligand side. The geometrical changes associated with this rotation are reflected in the absolute values of the Ni−C−C−C dihedral angle, 93 and 112° in **7** and **7′**, respectively, and 172° in the transition state (**TS$_{ROT}$**), indicating an upright conformation of the allyl ligand. This C3−C2 rotation of the η^1-allyl ligand corresponds to the rate-determining step of the syn−anti exchange experimentally detected by NMR and discussed above. In fact, once **7′** is formed, a η^1 to η^3 shift of the allyl group regenerates the square-planar reactant **6** with the hydrogen atoms in C3 exchanged. This last step is completely equivalent to the first one, **6** → **7**, discussed above. Interestingly, the activation energy for the entire process ($\Delta E^{\ddagger}$ = 23.1 kcal mol^{-1})[51] is higher than that associated with the rotation of the η^3-allyl about the Ni−η^3-allyl axis (Figure 4; 20.1 kcal mol^{-1}), indicating that syn−syn, anti−anti exchange should be more facile than syn−anti exchange, in good agreement with the experimental findings.

The possibility of a syn−syn, anti−anti exchange involving η^1-allyl intermediates (**7** and **7′**) was also investigated. Overall, this corresponds to a 180° rotation of η^3-allyl in the square-planar species **6**. Thus, the mechanism for such a process involving the participation of η^1 intermediates had to go first through a $\eta^3-\eta^1$ shift: that is, breaking of a Ni−C bond such as in **6** → **TSI** → **7** or in **6** → **TSI′** → **7′** (Figure 5). However, it should be noted that in both of these cases the Ni−C bond formed (and broken) is the one cis to the chloride ligand. Once this first $\eta^3-\eta^1$ shift is accomplished, the syn−syn, anti−anti exchange can only occur if the subsequent slippage from η^1 back to η^3 (from the T-shaped intermediates **7** and **7′**) corresponds to the formation of a Ni−C bond cis to the carbene ligand. However, a thorough search of the potential energy surface associated with this process did not provide a transition state, indicating that participation of η^1-allyl intermediates, such as **7** and **7′**, in syn−syn, anti−anti exchange is very unlikely to occur.

Conclusions

Neutral complexes of the type [Ni(η^3-C_3H_5)(Im)X] can be easily prepared from the cleavage reaction of the dimer [Ni(η^3-C_3H_5)Br]$_2$ with imidazol-2-ylidenes. The rotation of the carbene ligand is highly hindered for ^{t}Bu$_2$Im but considerably faster for Me_4Im and Me_2Im ($\Delta G^{\ddagger}$ = 14−18 kcal mol^{-1}). The increasing volume of the halogen atom enhances the $\Delta G^{\ddagger}$ value of the process.

At higher temperatures, complexes undergo further conformational exchange processes. At moderate temperatures, exchange between isomers is well explained through rotation of the allyl ligand in its own plane, about the Ni−η^3-allyl axis. At high temperatures, both NHC and allyl rotation processes take place simultaneously with a $\eta^3-\eta^1-\eta^3$ isomerization of the allyl group.

DFT calculations suggest an intramolecular path for rotation of the allyl ligand about the Ni−η^3-allyl bond, corresponding to a "spin-forbidden" process with participation of spin singlet and spin triplet species.

Experimental Section

General Considerations. All manipulations and reactions were carried out under an atmosphere of dinitrogen (<5 ppm of oxygen or water) using standard Schlenk vessel, vacuum-line, or drybox techniques. Solvents were predried over activated 4 Å molecular sieves and then distilled under an atmosphere of dinitrogen from sodium/benzophenone (diethyl ether, tetrahydrofuran, and toluene) or calcium hydride (*n*-hexane, dichloromethane) and stored under dinitrogen. Deuterated solvents (C_6D_6, toluene-d_8, CD_2Cl_2, 1,1,2,2-tetrachloroethane-d_2, and C_6D_5Br) for NMR samples were dried

(51) This corresponds to the electronic activation energy. The comparison has to be made in terms of energy ($\Delta E^{\ddagger}$) and not *free* energy ($\Delta G^{\ddagger}$), since the rate-limiting step for η^3-allyl rotation goes through MECP (Figure 4), which are not stationary points and, hence, standard frequency analysis is not applicable (see Computational Details).

with molecular sieves, degassed by freeze−pump−thaw cycles, and stored in ampules over activated molecular sieves. The NMR spectra were recorded on a Varian Unity 300 spectrometer (^{1}H, 300 MHz; ^{13}C, 75.43 MHz) and referenced internally using residual protio solvent (^{1}H) or solvent (^{13}C) resonances relative to tetramethylsilane (δ 0). Assignments were supported by one-dimensional nuclear Overhauser difference experiments, selective ^{1}H decoupling, and COSY and HETCOR two-dimensional correlations. The NMR data for compounds **1**−**5** are given at room temperature (ca. 295 K), except when specified. All chemical shifts are quoted in δ (ppm), and coupling constants are given in Hz. Multiplicities are abbreviated as follows: singlet (s), doublet (d), triplet (t), multiplet (m), broad (br), very (v). For complexes **2**−**5**, VT-NMR experiments were performed in toluene-d_8 containing a few drops of CD_2Cl_2 to increase solubility. NMR complete line-shape analyses were carried out using the gNMR software. Elemental analyses were performed on a Fisons Instrument Mod EA-1108 analyzer by the Laboratório de Análises at this Institute. Reagents such as potassium *tert*-butoxide were purchased from Aldrich and used as received. NaI was dried under vacuum at 100 °C for several hours. NaH was purchased as a 60% mineral oil dispersion, washed with THF, and dried under vacuum. Compounds such as [Ni(η-C_3H_5)Br]$_2$,[52] 1,3-dimethylimidazolium iodide,[53] 1,3,4,5-tetramethylimidazol-2-ylidene,[26] and 1,3-di-*tert*-butylimidazol-2-ylidene[26] were prepared according to literature methods.

Synthesis of [Ni(η^3-C_3H_5)(^{t}Bu$_2$Im)Br] (1). A solution of 1,3-di-*tert*-butylimidazol-2-ylidene (0.36 g, 2.0 mmol) in THF (15 mL) was added dropwise to a dark red solution of [Ni(η^3-C_3H_5)Br]$_2$ (0.39 g, 1.08 mmol) in THF (15 mL), at −50 °C. The solution was warmed to 0 °C over 6.5 h, with stirring. The ethanol cold bath was removed, and the cloudy orange solution obtained was warmed to room temperature and stirred for another 10 min. The solvent was removed under vacuum and the residue washed with hexane. An orange solution was extracted with toluene (20 mL), and 100 mL of hexane was added with stirring, leading to the precipitation of a microcrystalline orange powder. Further recrystallization in cold diethyl ether (−20 °C) gave crystals of **1** suitable for X-ray diffraction. Yield: 0.64 g (89%). Anal. Calcd for $C_{14}H_{25}N_2NiBr$: C, 46.71; H, 7.00; N, 7.78. Found: C, 46.89; H, 7.05; N, 7.62. ^{1}H NMR (C_6D_6): δ 6.61 (s, H6, 1H); 6.54 (s, H5, 1H); 5.01 (m, $^3J_{HH}$ = 6.6 Hz, H2^{meso}, 1H); 3.72 (m, $^3J_{HH}$ = 6.0 Hz, H1^{syn}, 1H); 2.86 (m, $^3J_{HH}$ = 13.8 Hz, H1^{anti}, 1H); 2.32 (m, $^3J_{HH}$ = 6.0 Hz, H3^{syn}, 1H); 1.90 (s, C(CH_3)$_3$ from C11, 9H); 1.63 (s, C(CH_3)$_3$ from C7, 9H); 1.28 (m, $^3J_{HH}$ = 12.0 Hz, H3^{anti}, 1H). ^{13}C{^{1}H} NMR (C_6D_6): δ 179.0 (C4); 119.3 (C5); 119.2 (C6); 105.2 (C2); 64.5 (C1); 58.5 (C11); 58.2 (C7); 46.1 (C3); 32.0 (C(*C*H$_3$)$_3$ from C11); 31.6 (C(*C*H$_3$)$_3$ from C7).

Synthesis of [Ni(η^3-C_3H_5)(Me_4Im)Br] (2). A solution of 1,3,4,5-tetramethylimidazol-2-ylidene (0.25 g, 2.0 mmol) in THF (10 mL) was added dropwise to a dark red solution of [Ni(η^3-C_3H_5)Br]$_2$ (0.35 g, 0.98 mmol) in THF (10 mL), at −50 °C. The solution was stirred for 3.5 h and slowly warmed to 0 °C. At this point, the cold ethanol bath was removed and the mixture was stirred for another 10 min. The turbid orange solution was filtered, and the solvent was evaporated under vacuum. The residue was washed with hexane, which dissolved also a small amount of the reaction product (recovered by concentration of the solution and cooling it down to −80 °C). The solid was further extracted with toluene. The solution was concentrated and cooled to −80 °C, leading to the precipitation of an orange powder, corresponding to the desired compound **2**. Yield: 0.47 g (79%). Anal. Calcd for $C_{10}H_{17}N_2NiBr$: C, 39.53; H, 5.64; N, 9.22. Found: C, 39.03; H, 5.95; N, 8.76. ^{1}H NMR (C_6D_6): δ 5.01 (m, $^3J_{HH}$ = 6.9 Hz, H2^{meso}, 1H); 3.86 (m, $^3J_{HH}$ = 7.2 Hz, H1^{syn}, 1H); 3.58 (br s, NCH_3 from C5, 3H); 3.13 (br s, NCH_3 from C4, 3H); 2.86 (m, $^3J_{HH}$ = 14.4 Hz, H1^{anti}, 1H); 2.33 (m, $^3J_{HH}$ = 6.3 Hz, H3^{syn}, 1H); 1.58 (m, $^3J_{HH}$ = 12.9 Hz, H3^{anti}, 1H); 1.29 (br s, CCH_3, 3H); 1.27 (br s, CCH_3, 3H). ^{1}H NMR (CD_2Cl_2): δ 5.27 (m, $^3J_{HH}$ = 7.2 Hz, H2^{meso}, 1H); 4.03 (s, NCH_3 from C5, 3H); 3.65 (m, $^3J_{HH}$ = 7.2 Hz, H1^{syn}, 1H); 3.64 (s, NCH_3 from C4, 3H); 3.46 (m, $^3J_{HH}$ = 5.7 Hz, H3^{syn}, 1H); 2.58 (m, $^3J_{HH}$ = 13.8 Hz, H1^{anti}, 1H); 2.09 (s, CCH_3, 3H); 2.04 (s, CCH_3, 3H); 1.78 (m, $^3J_{HH}$ = 12.9 Hz, H3^{anti}, 1H). ^{1}H NMR (toluene-d_8, 215 K): δ 5.02 (m, $^3J_{HH}$ = 6.6 Hz, H2^{meso}, 1H); 3.72 (m, $^3J_{HH}$ = 6.9 Hz, H1^{syn}, 1H); 3.57 (s, NCH_3 from C5, 3H); 3.12 (s, NCH_3 from C4, 3H); 2.74 (m, $^3J_{HH}$ = 14.1 Hz, H1^{anti}, 1H); 2.34 (m, $^3J_{HH}$ = 6.6 Hz, H3^{syn}, 1H); 1.58 (m, $^3J_{HH}$ = 13.2 Hz, H3^{anti}, 1H); 1.34 (s, CCH_3, 3H); 1.32 (s, CCH_3, 3H). ^{13}C{^{1}H} NMR (C_6D_6): δ 179.5 (C4); 126.0 (C5 or C6); 124.9 (C6 or C5); 106.8 (C2); 67.6 (C1); 44.7 (C3); 34.6 (C9 or C10); 34.0 (C9 or C10); 8.1 (C7 and C8). ^{13}C{^{1}H} NMR (CD_2Cl_2): δ 178.0 (C4); 126.1 (C5 or C6); 125.9 (C6 or C5); 107.7 (C2); 67.3 (C1); 45.6 (C3); 35.2 (C9 or C10); 34.6 (C10 or 9); 9.0 (C7 and C8).

Synthesis of [Ni(η^3-C_3H_5)(Me_2Im)Br] (3). In a degassed Schlenk tube, 1,3-dimethylimidazolium iodide (0.86 g, 3.8 mmol) and NaH (0.105 g, 4.4 mmol) were weighed, and a catalytic amount of KO^{t}Bu was added. The Schlenk tube was immersed in a −80 °C ethanol bath, and 50 mL of THF was added. The mixture was stirred for 2 h, and then the cold bath was removed. After 2.5 h, no further hydrogen evolution was observed and the solvent was evaporated under vacuum, yielding a yellow oil. Hot toluene (65 °C) was added and the resulting mixture stirred. The colorless solution was filtered into a cold toluene solution (−50 °C) of [Ni(η^3-C_3H_5)Br]$_2$ (0.45 g, 1.26 mmol), immediately precipitating an orange powder. The mixture was stirred in the cold bath for 2 h. At this point, the cold bath was removed and the solution was slowly warmed, for 30 min. The solution was filtered and the remaining orange powder extracted with toluene. The solvent was pumped out and the residue washed with hexane. One portion of the solid was extracted with toluene and cooled to −20 °C, yielding 0.22 g of a microcrystalline orange powder. The remaining solid was extracted with THF and double-layered with hexane at −20 °C, yielding pale orange crystals. Yield: 0.29 g (72%). Anal. Calcd for $C_8H_{13}N_2NiBr$: C, 34.84; H, 4.75; N, 10.16. Found: C, 34.80; H, 4.17; N, 9.76. ^{1}H NMR (C_6D_6): 5.86 (s, H5 and H6, 2H); 4.95 (m, $^3J_{HH}$ = 6.9 Hz, H2^{meso}, 1H); 3.85 (m, $^3J_{HH}$ = 6.9 Hz, H1^{syn}, 1H); 3.39 (v br, CH_3); 3.18 (v br, CH_3); 2.80 (m, $^3J_{HH}$ = 14.1 Hz, H1^{anti}, 1H); 2.23 (m, $^3J_{HH}$ = 6.9 Hz, H3^{syn}, 1H); 1.47 (m, $^3J_{HH}$ = 12.9 Hz, H3^{anti}, 1H). ^{1}H NMR (toluene-d_8): 5.97 (s, H5 and H6, 2H); 4.95 (m, $^3J_{HH}$ = 6.9 Hz, H2^{meso}, 1H); 3.67 (m, $^3J_{HH}$ = 6 Hz, H1^{syn}, 1H); ca. 3.39 (br, CH_3, 6H); 2.66 (m, $^3J_{HH}$ = 14.1 Hz, H1^{anti}, 1H); 2.27 (m, $^3J_{HH}$ = 6.6 Hz, H3^{syn}, 1H); 1.47 (m, $^3J_{HH}$ = 12.6 Hz, H3^{anti}, 1H). ^{1}H NMR (toluene-d_8, 215 K): 5,82 (s, H5 or H6, 1H); 5,76 (s, H5 or H6, 1H); 4.93 (m, $^3J_{HH}$ = 6.6 Hz, H2^{meso}, 1H); 3.76 (d, $^3J_{HH}$ = 6.6 Hz, H1^{syn} or H3^{syn}, 1H); 3.47 (s, CH_3, 3H); 3.04 (s, CH_3, 3H); 2.72 (d, $^3J_{HH}$ = 14.1 Hz, H1^{anti} or H3^{anti}, 1H); 2.21 (m, $^3J_{HH}$ = 6.6 Hz, H1^{syn} or H3^{syn}, 1H); 1.46 (d, $^3J_{HH}$ = 12.9 Hz, H1^{anti} or H3^{anti}, 1H). ^{1}H NMR (toluene-d_8, 342 K): 6.05 (s, H5 and H6, 2H); 4.96 (br m, H2^{meso}, 1H); 3.64 (br, H1^{syn}, 1H); 3.43 (br, CH_3, 6H); 2.64 (br m, $^3J_{HH}$ = 13.8 Hz, H1^{anti}, 1H); 2.29 (br, H3^{syn}, 1H); 1.48 (br m, $^3J_{HH}$ = 10.8 Hz, H3^{anti}, 1H). ^{13}C{^{1}H} NMR (C_6D_6): 179.5 (C4); 122.7 (C5 and C6); 108.1 (C2); 67.7 (C1); 46.0 (C3); 37.7 (br, CH_3). ^{13}C{^{1}H} NMR (CD_2Cl_2): C4 missing; 122.7 (C5 and C6); 108.1 (C2); 67.7 (C1); 46.0 (C3); 37.7 (br, CH_3).

Synthesis of [Ni(η^3-C_3H_5)(Me_2Im)I] (4). 1,3-Dimethylimidazolium iodide (0.59 g, 2.7 mmol), NaH (0.07 g, 2.9 mmol), and a catalytic amount of KO^{t}Bu were weighed in a degassed Schlenk tube and placed in a −80 °C ethanol/liquid N_2 bath. THF (30 mL) was added and the mixture stirred for 1 h. The cold bath was then removed and the solution warmed to room temperature, with stirring for a further 2 h. The yellow solution thus obtained was filtered dropwise over [Ni(η^3-C_3H_5)Br]$_2$ (0.43 g, 1.2 mmol), at −50 °C. The mixture was stirred for 2 h in the cold bath and then warmed

(52) Semmelhack, M. F.; Helquist, P. M. *Org. Synth.* **1972**, *52*, 115.
(53) Arduengo, A. J., World Patent WO9114678 5, Oct 3, 1991.

for 1 h. The orange solution was filtered, concentrated, and cooled to −20 °C, resulting in the formation of orange crystals of compound **4**. Further recrystallization of the compound in cold toluene yielded suitable crystals for X-ray diffraction. Yield: 0.60 g (78%). Anal. Calcd for $C_8H_{13}N_2NiI$: C, 29.77; H, 4.06; N, 8.08. Found: C, 29.68; H, 3.94; N, 8.49. ^{1}H NMR (C_6D_6): δ 5.87 (s, H5 or H6, 1H); 5.81 (s, H5 or H6, 1 H); 4,80 (m, $^3J_{HH}$ = 6.0 Hz, H2^{meso}, 1H); 3.90 (m, $^3J_{HH}$ = 7.2 Hz, H1^{syn}, 1H); 3.37 (s, CCH_3, 3H); 3.01 (s, CCH_3, 3H); 2.57 (m, H3^{syn}, 1H); 2.53 (m, $^3J_{HH}$ = 14.7 Hz, H1^{anti}, 1H); 1.58 (m, $^3J_{HH}$ = 12.9 Hz, H3^{anti}, 1H). ^{1}H NMR (toluene-d_8): δ 6.07 (s, H5 or H6, 1H); 6.01 (s, H5 or H6, 1 H); 4.82 (m, $^3J_{HH}$ = 7.2 Hz, H2^{meso}, 1H); 3.69 (m, $^3J_{HH}$ = 7.5 Hz, H1^{syn}, 1H); 3.49 (s, CCH_3, 3H); 3.14 (s, CCH_3, 3H); 2.63 (m, $^3J_{HH}$ = 7.2 Hz, H3^{syn}, 1H); 2.38 (m, $^3J_{HH}$ = 14.7 Hz, H1^{anti}, 1H); 1.60 (m, $^3J_{HH}$ = 13.2 Hz, H3^{anti}, 1H). ^{13}C{^{1}H} NMR (C_6D_6): C4 missing; 122.1 (C5 or C6); 121.7 (C5 or C6); 106.0 (C2); 65.5 (C1); 49.8 (C3); 37.2 (br, C7 or C8); 36.5 (br, C7 or C8). ^{13}C{^{1}H} NMR (toluene-d_8): C4 missing; 122.3 (C5 or C6); 122.0 (C5 or C6); 106.2 (C2); 65.4 (C1); 50.0 (C3); 37.3 (br, C7 or C8); 36.6 (br, C7 or C8).

Synthesis of [Ni(η^3-C_3H_5)(Me_4Im)I] (5). Equimolar amounts of [Ni(η^3-C_3H_5)(Me_4Im)Br] (**2**) (0.13 g, 0.42 mmol) and NaI (0.07 g, 0.46 mmol) were weighed in a Schlenk tube. THF (15 mL) was added and the mixture stirred for 12 h. The solvent was evaporated under vacuum and the residue extracted with toluene. The solution was double-layered with hexane and stored at −20 °C, giving 0.13 g of orange crystals corresponding to a mixture of the title compound **5** (66% yield determined by ^{1}H NMR at 216 K) and unreacted [Ni(η^3-C_3H_5)(Me_4Im)Br] (**2**). The solids were redissolved in THF (10 mL), and a small excess of NaI (0.015 g, 0.10 mmol), relative to the contamination of bromide compound **2**, was added. The mixture was stirred for 36 h. The solvent was then evaporated under vacuum. Further extraction with toluene, double-layering with hexane, and storage at −20 °C gave orange crystals suitable for X-ray diffraction of pure compound **5**. Yield: 0.06 g (90% relative to the amount of solid obtained in the first recrystallization). Anal. Calcd for $C_{10}H_{17}N_2NiI$: C, 34.23; H, 4.88; N, 7.98. Found: C, 34.23; H, 4.81; N, 7.85. ^{1}H NMR (C_6D_6): δ 4.90 (m, $^3J_{HH}$ = 6.9 Hz, H2^{meso}, 1H); 3.90 (d, $^3J_{HH}$ = 6.6 Hz, H1^{syn}, 1H); 3.47 (s, NCH_3 from C5, 3H); 3.09 (s, NCH_3 from C4, 3H); 2.68 (d, $^3J_{HH}$ = 6.6 Hz, H3^{syn}, 1H); 2.59 (d, $^3J_{HH}$ = 14.4 Hz, H1^{anti}, 1H); 1.70 (d, $^3J_{HH}$ = 12.9 Hz, H3^{anti}, 1H); 1.31 (s, CCH_3, 3H); 1.28 (s, CCH_3, 3H). ^{1}H NMR (toluene-d_8): δ 4.89 (m, $^3J_{HH}$ = 6.6 Hz, H2^{meso}, 1H); 3.69 (d, $^3J_{HH}$ = 7.5 Hz, H1^{syn}, 1H); 3.53 (s, NCH_3 from C5, 3H); 3.17 (s, NCH_3 from C4, 3H); 2.69 (d, $^3J_{HH}$ = 6.9 Hz, H3^{syn}, 1H); 2.42 (d, $^3J_{HH}$ = 14.1 Hz, H1^{anti}, 1H); 1.69 (d, $^3J_{HH}$ = 12.6 Hz, H3^{anti}, 1H); 1.47 (s, CCH_3, 3H); 1.44 (s, CCH_3, 3H). ^{13}C{^{1}H} NMR (C_6D_6): δ 179.4 (C4); 125.5 (C5 or C6); 125.3 (C6 or C5); 105.9 (C2); 65.2 (C1); 49.8 (C3); 34.8 (C9 or C10); 34.1 (C9 or C10); 8.33 (C7 or C8); 8.26 (C7 or C8). ^{13}C{^{1}H} NMR (toluene-d_8, 192 K): δ 177.1 (C4); 125.4 (C5 or C6); 125.0 (C6 or C5); 106.0 (C2); 64.8 (C1); 50.6 (C3); 34.6 (C9 or C10); 33.8 (C9 or C10); 8.2 (C7 and C8).

X-ray Experimental Data. Crystallographic and experimental details of crystal structure determinations are given in Table 6. Suitable crystals of complex **1** were mounted on a capillary, and data were collected at room temperature on an Enraf-Nonius MACH3 diffractometer equipped with Mo radiation. For compounds **2**, **4**, and **5**, crystals were selected under an inert atmosphere, covered with polyfluoroether oil, and mounted on a nylon loop. Since crystals of **2** were extremely small and diffracted weakly, synchrotron radiation was used to collect diffraction data on this compound. Data were collected at Station 9.8, Daresbury SRS, Daresbury, U.K., using a Bruker SMART CCD diffractometer at 150 K. Complex **4** also yielded weakly diffracting crystals whose data were collected at 180 K on a Nonius KappaCCD diffractometer with graphite-monochromated Mo Kα radiation. Images of **2** and **4** were processed with the DENZO and SCALEPACK programs.[54] In the case of complex **5**, the data were collected at 130 K on a Bruker AXS-KAPPA APEX II diffractometer using graphite-monochromated Mo Kα radiation. For complexes **1** and **5**, solutions were found with direct methods using SIR97[55] and refined using SHELXL[56] included in the package of programs WINGX, Version 1.70.01.[57] For both **2** and **4**, structures were solved by direct methods using the program SIR92,[58] and refinements (on *F*) and graphical calculations were performed using the CRYSTALS[59] program suite. For compound **5**, a certain extent of disorder is observed for atom C2 (with 60% and 30% probability), and also some residual electron density is detected near atom C1 (that could not be modeled).

Table 6. Crystal Data and Structure Refinement Details for Complexes 1, 2, 4, and 5

	1	**2**	**4**	**5**
formula	$C_{14}H_{25}BrN_2Ni$	$C_{10}H_{17}BrN_2Ni$	$C_8H_{13}N_2INi$	$C_{10}H_{17}N_2INi$
M_r	359.98	303.87	322.82	350.87
λ/Å	0.71069	0.6923	0.71069	0.71069
T (K)	293(2)	150(2)	180(2)	130(2)
cryst syst	orthorhombic	monoclinic	monoclinic	triclinic
space group	$Pbn2_1$	$C2/c$	$P2_1/m$	$P\bar{1}$
a (Å)	9.686(3)	20.265(5)	7.2153(19)	7.9820(9)
b (Å)	11.236(3)	8.471(2)	8.362(2)	8.8620(10)
c (Å)	14.713(3)	14.144(4)	9.324(3)	10.303(2)
α (deg)				112.019(2)
β (deg)		93.703(4)	103.351(12)	100.553(2)
γ (deg)				102.160(2)
V (Å^3)	1601.2(1)	2423.0(11)	547.4(3)	632.2(2)
Z	4	8	2	2
ρ_{calcd} (g cm^{-3})	1.493	1.666	1.959	1.843
μ (mm^{-1})	3.694	4.865	4.545	3.943
θ_{max} (deg)	25.97	30	27	41.3
total no. of data	1626	3558	1786	11 785
unique no. of data	1626	2769	960	6541
R_{int}	0.00	0.033	0.086	0.0235
R ($I > 3\sigma(I)$)	0.063	0.0345	0.1451	0.0319
R_w	0.078	0.0434	0.1286	0.0744
goodness of fit	0.945	1.0257	1.2114	1.05
Flack param	0.03(3)			
ρ_{min}	−0.449	−0.65	−2.08	−2.35
ρ_{max}	0.464	2.24	4.76	2.54

For **4**, the low quality of the crystal accounts for the relatively poor quality of the diffraction data. This complex is disordered over a mirror plane. There may also be substitutional disorder of the iodine and allyl group, which might account for the rather high residual electron density. Geometric and vibrational similarity restraints were applied. Data were also collected using synchrotron radiation; however, the quality of the solution did not improve and ultimately the KCCD-collected data were used in the refinement.

Hydrogen atoms in compound **1** were inserted in idealized positions riding on the parent carbon atoms. For both **2** and **4** the non-hydrogen atoms were refined with anisotropic displacement

(54) Otwinowski, Z.; Minor, W. In *Methods in Enzymology*; Carter, C. N., Jr., Sweet, R. M., Eds.; Academic Press: New York, 1996; p 276.
(55) SIR97: Altomare, A.; Burla, M. C.; Camalli, M.; Cascarano, G. L.; Giacovazzo, C.; Guagliardi, A.; Moliterni, A. G. G.; Polidori, G.; Spagna, R. *J. Appl. Crystallogr.* **1999**, *32*, 115.
(56) Sheldrick, G. M. SHELX97-Programs for Crystal Structure Analysis (Release 97-2); Institüt für Anorganische Chemie der Universität, Tammanstrasse 4, D-3400 Göttingen, Germany, 1998.
(57) Farrugia, L. J. *J. Appl. Crystallogr.* **1999**, *32*, 837.
(58) SIR92: Altomare, A.; Cascarano, G. L.; Giacovazzo, C.; Guagliardi, A. *J. Appl. Crystallogr.* **1993**, *26*, 343.
(59) (a) Watkin, D. J.; Prout, C. K.; Carruthers, J. R.; Betteridge, P. W. CRYSTALS; Oxford, U.K., 1996. (b) P. W. Betteridge, P. W.; Carruthers, J. R.; Cooper, R. I.; Prout, K.; Watkin, D. J. *J. Appl. Crystallogr.* **2003**, *36*, 1487. (c) Watkin, D. J.; Prout, C. K.; Pearce, L. J. CAMERON; Oxford, U.K., 1996.

parameters. Hydrogen atoms were located in Fourier maps and their positions adjusted geometrically (after each cycle of refinement) with isotropic thermal parameters. Chebychev weighting schemes and empirical absorption corrections were applied in each case.[60] In compound **5** all hydrogen atoms were found in the difference Fourier map and refined freely. In this case, the hydrogen atoms of the allyl terminal carbons (C1 and C3) were inserted in idealized positions and once again refined in the parent carbon atom.

Figures were generated using ORTEP3.[61] Data were deposited at the CCDC under the deposit numbers 603290 for **1**, 602970 for **2**, 602971 for **4**, and 603289 for **5**.

Computational Details. All calculations were performed using the Gaussian 98 software package[62] and the B3LYP hybrid functional, without symmetry constraints. That functional includes a mixture of Hartree−Fock[63] exchange with DFT[44] exchange correlation, given by Becke's three-parameter functional[64] with the Lee, Yang, and Parr correlation functional, which includes both local and nonlocal terms.[65,66] The basis set used consisted of LanL2DZ[67] augmented with an f-polarization function[68] for Ni, the same basis augmented with a d-polarization function[69] for the halogens, and a standard 6-31G(d,p) set[70] for the remaining elements. Transition state optimizations were performed with the synchronous transit-guided quasi-Newton method (STQN) developed by Schlegel et al.[71] Frequency calculations were performed to confirm the nature of the stationary points, yielding one imaginary frequency for the transition states and none for the minima. Each transition state was further confirmed by following its vibrational mode downhill on both sides and obtaining the minima presented on the energy profile. The minimum energy crossing points (MECP) between the spin singlet ($S = 0$) and the spin triplet ($S = 1$) potential energy surfaces (PES) were determined using a code developed by Harvey et al.[72] This code consists of a set of shell scripts and Fortran programs that uses the Gaussian results of energies and gradients of both spin states to produce an effective gradient pointing toward the MECP. Spin contamination was carefully monitored for all the unrestricted calculations, and the values of $\langle S^2 \rangle$ indicate minor spin contamination and are presented as Supporting Information. The energy values for allyl rotation are not zero point corrected since, on one hand, the maximum deviation between the zero point corrected and the uncorrected energies is 0.8 kcal mol^{-1}, with all stationary points considered, and, on the other, MECP are not stationary points and a standard frequency analysis is not applicable.[72] The free energies referred to in the text were obtained at 298.15 K and 1 atm by conversion of the zero point corrected electronic energies with the thermal energy corrections based on the calculated structural and vibrational frequency data. A natural population analysis (NPA)[48] and the resulting Wiberg indices[46] were used for a detailed study of the electronic structure and bonding of the optimized species.

The most accurate functional to describe energy differences between states of different spin in organo-transition-metal complexes is still a matter of discussion. Although the hybrid functionals, such as B3LYP, can be a good choice in many cases, their 20% admixture of exact exchange may overestimate the stability of higher spin states in some systems. Modified hybrid functionals with 15% exact exchange (B3LYP*) have been proposed, specially for first-row transition-metal complexes.[73,74] The dependence of the system studied, [Ni(η^3-C_3H_5)(Me_2Im)Cl], on the amount of exact exchange included in the functional was investigated. The energy profile associated with the allyl rotation was recalculated using B3LYP*. The MECP were reoptimized with the modified functional, and single-point energy calculations with B3LYP* were performed on the geometries optimized with B3LYP for the stationary points. The activation energy obtained with B3LYP* is only 1.6 kcal mol^{-1} higher than the B3LYP energy, showing only a minimal dependence of the system studied on the amount of exact exchange included in the functional. B3LYP values are presented in the text, since the corresponding activation energy is a better match to the experimental value. The complete energy profile with B3LYP* energies is presented in the Supporting Information (Figure 13 of the Supporting Information).

Acknowledgment. We thank the Fundação para a Ciência e Tecnologia for financial support (Projects POCTI/QUI/42015/2001 and POCI/QUI/59025/2004, cofinanced by the FEDER) and for a fellowship (SFRH/BD/9127/2002, to L.C.S.) and the Royal Society (S.I.P.) for a University Research Fellowship.

Note Added after ASAP Publication. In the version of this paper published on the Web on July 27, 2006, references 17−19 were incorrect. In the version of the paper that now appears, these references are correct.

Supporting Information Available: Figures giving relevant NMR spectra, CIF files giving X-ray structural data, including data collection parameters, positional and thermal parameters, and bond distances and angles for complexes **1**, **2**, **4**, and **5**, and tables of atomic coordinates for all the optimized species and the energy profile for allyl rotation obtained with B3LYP*. This material is available free of charge via the Internet at http://pubs.acs.org.

OM060444P

(60) Walker, N.; Stuart, D. *Acta Crystallogr., Sect. A* **1983**, *39*, 158.
(61) ORTEP3 for Windows: Farrugia, L. J. *J. Appl. Crystallogr.* **1997**, *30*, 565.
(62) Frisch, M. J.; Trucks, G. W.; Schlegel, H. B.; Scuseria, G. E.; Robb, M. A.; Cheeseman, J. R.; Zakrzewski, V. G.; Montgomery, J. A., Jr.; Stratmann, R. E.; Burant, J. C.; Dapprich, S.; Millam, J. M.; Daniels, A. D.; Kudin, K. N.; Strain, M. C.; Farkas, O.; Tomasi, J.; Barone, V.; Cossi, M.; Cammi, R.; Mennucci, B.; Pomelli, C.; Adamo, C.; Clifford, S.; Ochterski, J.; Petersson, G. A.; Ayala, P. Y.; Cui, Q.; Morokuma, K.; Malick, D. K.; Rabuck, A. D.; Raghavachari, K.; Foresman, J. B.; Cioslowski, J.; Ortiz, J. V.; Stefanov, B. B.; Liu, G.; Liashenko, A.; Piskorz, P.; Komaromi, I.; Gomperts, R.; Martin, R. L.; Fox, D. J.; Keith, T.; Al-Laham, M. A.; Peng, C. Y.; Nanayakkara, A.; Gonzalez, C.; Challacombe, M.; Gill, P. M. W.; Johnson, B. G.; Chen, W.; Wong, M. W.; Andres, J. L.; Head-Gordon, M.; Replogle, E. S.; Pople, J. A. *Gaussian 98*, revision A.7; Gaussian, Inc.: Pittsburgh, PA, 1998.
(63) Hehre, W. J.; Radom, L.; Schleyer, P. v. R.; Pople, J. A. *Ab Initio Molecular Orbital Theory*; Wiley: New York, 1986.
(64) Becke, A. D. *J. Chem. Phys.* **1993**, *98*, 5648.
(65) Miehlich, B.; Savin, A.; Stoll, H.; Preuss, H. *Chem. Phys. Lett.* **1989**, *157*, 200.
(66) Lee, C.; Yang, W.; Parr, G. *Phys. Rev. B* **1988**, *37*, 785.
(67) (a) Dunning, T. H., Jr.; Hay, P. J. In *Modern Theoretical Chemistry*; Schaefer, H. F., III, Ed.; Plenum: New York, 1976; Vol. 3, p 1. (b) Hay, P. J.; Wadt, W. R. *J. Chem. Phys.* **1985**, *82*, 270. (c) Wadt, W. R.; Hay, P. J. *J. Chem. Phys.* **1985**, *82*, 284. (d) Hay, P. J.; Wadt, W. R. *J. Chem. Phys.* **1985**, *82*, 2299.
(68) Ehlers, A. W.; Böhme, M.; Dapprich, S.; Gobbi, A.; Höllwarth, A.; Jonas, V.; Köhler, K. F.; Stegmann, R.; Veldkamp, A.; Frenking, G. *Chem. Phys. Lett.* **1993**, *208*, 111.
(69) Höllwarth, A.; Böhme, M.; Dapprich, S.; Ehlers, A. W.; Gobbi, A.; Jonas, V.; Köhler, K. F.; Stegmann, R.; Veldkamp, A.; Frenking, G. *Chem. Phys. Lett.* **1993**, *208*, 237.
(70) (a) Ditchfield, R.; Hehre, W. J.; Pople, J. A. *J. Chem. Phys.* **1971**, *54*, 724. (b) Hehre, W. J.; Ditchfield, R.; Pople, J. A. *J. Chem. Phys.* **1972**, *56*, 2257. (c) Hariharan, P. C.; Pople, J. A. *Mol. Phys.* **1974**, *27*, 209. (d) Gordon, M. S. *Chem. Phys. Lett.* **1980**, *76*, 163. (e) Hariharan, P. C.; Pople, J. A. *Theor. Chim. Acta* **1973**, *28*, 213.
(71) (a) Peng, C.; Ayala, P. Y.; Schlegel, H. B.; Frisch, M. J. *J. Comput. Chem.* **1996**, *17*, 49. (b) Peng, C.; Schlegel, H. B. *Isr. J. Chem.* **1994**, *33*, 449.
(72) Harvey, J. N.; Aschi, M.; Schwarz, H.; Koch, W. *Theor. Chem. Acc.* **1998**, *99*, 95.
(73) Harvey, J. N. *Struct. Bonding* **2004**, *112*, 151.
(74) Harvey, J. N.; Aschi, M. *Faraday Discuss.* **2003**, *124*, 129.